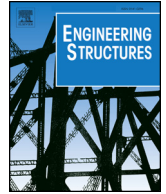


ELSEVIER

Contents lists available at ScienceDirect

Engineering Structures

journal homepage: [www.elsevier.com/locate/engstruct](http://www.elsevier.com/locate/engstruct)

# Optimal design of multiple damped-outrigger system incorporating buckling-restrained braces

Pao-Chun Lin<sup>a</sup>, Toru Takeuchi<sup>a,\*</sup>, Ryota Matsui<sup>b</sup>

<sup>a</sup> Tokyo Institute of Technology, Department of Architecture and Building Engineering, Ookayama 2-12-1, Meguro-ku, Tokyo 152-8550, Japan

<sup>b</sup> Hokkaido University, Department of Architectural and Structural Design, Kita 13-Nishi 8, Kita-ku, Sapporo, Hokkaido 060-8628, Japan

## ARTICLE INFO

### Keywords:

Outrigger  
Buckling-restrained brace  
Parametric study  
Optimal design  
Spectral analysis

## ABSTRACT

The outrigger system is an effective solution in mitigating seismic responses of core-tube-type tall buildings by mobilizing the axial stiffness of the perimeter columns. The concept of damped-outrigger has been proposed which introduces dampers in the outrigger system to dissipate seismic energy. This study investigates the seismic behavior of a damped-outrigger system incorporating buckling-restrained brace (BRB-outrigger). The outrigger effect combined with the energy dissipation mechanism of the buckling-restrained brace (BRB) effectively reduce the seismic response of the building. This study proposes the methods to evaluate the inelastic seismic response of structures with multiple damped-outriggers based on a spectral analysis (SA) procedure. For the structure with BRB-outriggers, the optimal outrigger elevations, and the relationships between the axial stiffness of the BRB, the axial stiffness of the perimeter column, and the flexural rigidity of the core structure in order to minimize the seismic response are the primary research objectives of this study. Analytical models with building heights of 64 m, 128 m, 256 m, and 384 m are used to perform the SA and the nonlinear response history analysis. This study concludes with a design recommendation for preliminary design purposes.

## 1. Introduction

The outrigger system has been an effective and economical solution for slender core-tube-type tall buildings in mitigating seismic responses and has been widely used as a seismic resistance system in tall buildings worldwide [1]. In the conventional outrigger systems, the outrigger truss connects the perimeter column to a relatively stiff core structure. When lateral loads, such as seismic or wind loads, are applied to the building, the outrigger system applies a resisting moment on the core structure by mobilizing the axial stiffness of the perimeter columns. The outrigger system is found to effectively reduce the roof drift, inter-story drift, and bending moment of the core structure by increasing the stiffness of the system [2]. However, the elastic design concept of the conventional outrigger could result in excessive force demands on outrigger members and perimeter columns, which increases difficulties and costs in engineering practices [3].

In order to avoid the excessive force demands in the conventional outrigger members and to implement energy dissipation mechanisms into the outrigger system, the concept of the damped-outrigger was proposed by inserting dampers between the outrigger truss end and the perimeter column [4]. The dampers dissipate energy through the relative movement between the outrigger truss end and the perimeter

column. The optimal outrigger elevations, and the relationships between the damper size, the axial stiffness of the perimeter column, and the flexural rigidity of the core structure in order to maximize the system damping ratio were investigated using complex eigenvalue analysis [5,6]. In addition, the study [7] reported the damped-outrigger system using the dynamic stiffness method, which is feasible for buildings with more than two outriggers. The study [5] reported that the optimal elevation of a single damped-outrigger incorporating viscous dampers ranges from 50% to 80% of the building height. The seismic performances of buildings with multiple outriggers were also studied. The study [8] reported the optimal single damped-outrigger elevation to be approximately 70% to 80% of the building height. In addition, placing a conventional and damped-outrigger at elevations of 70% and 50% of the building height, respectively, is effective in reducing structural damages. The study [9] reported that the overturning moment at the core structure base can be reduced when one of the multiple outriggers is close to the building foundation. The study [10] investigated the optimal damped-outrigger elevations when viscous damper and BRB are incorporated, and indicated that the optimal positions of the damped-outrigger with BRB and viscous damper are at the 7th and 5th zone, respectively, based on the 9-zone model structure. The damped-outrigger systems incorporating viscous dampers have

\* Corresponding author.

E-mail addresses: [lin.p.ab@m.titech.ac.jp](mailto:lin.p.ab@m.titech.ac.jp) (P.-C. Lin), [takeuchi.t.ab@m.titech.ac.jp](mailto:takeuchi.t.ab@m.titech.ac.jp) (T. Takeuchi), [ryota.matsui@eng.hokudai.ac.jp](mailto:ryota.matsui@eng.hokudai.ac.jp) (R. Matsui).

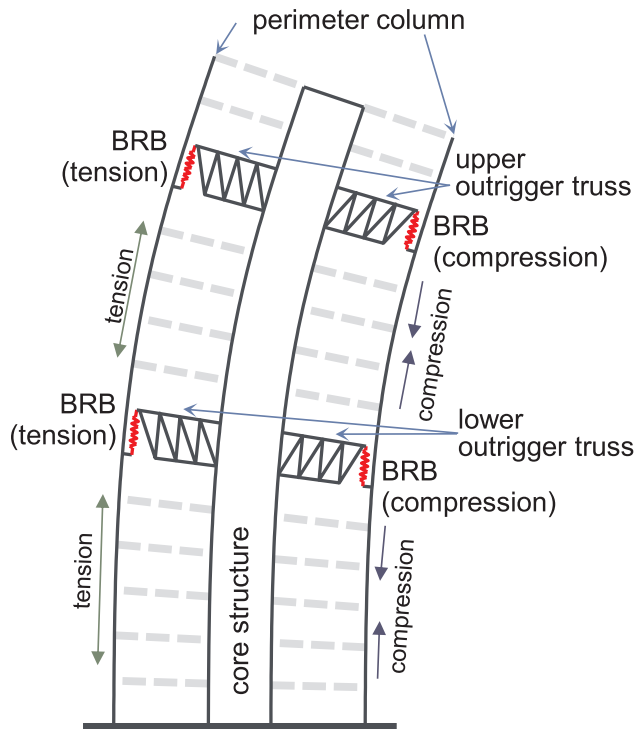


Fig. 1. Deformed dual BRB-outrigger system.

been utilized in actual construction projects to reduce the wind load effect [11]. In addition, buckling-restrained brace (BRB) [12] have been used as outrigger truss members in order to prevent excessive force demands on adjacent members in real construction project [13]. Most of the optimal multiple outrigger elevations in the past studies were determined from the combinations of several pre-selected possible elevations. The continuous seismic response distributions with respect to the changes of outrigger elevations have not been demonstrated.

This study reported the seismic behavior of a multiple-outrigger system incorporating BRB as energy dissipation device (BRB-outrigger). Fig. 1 shows the deformed structure with two BRB-outriggers (dual BRB-outrigger system). The core structure provides the majority of the lateral force resistance capacity. Each of the BRBs is arranged vertically between the outrigger truss ends and perimeter columns, so that the axial deformation demand of the BRB could be maximized. As shown in Fig. 1, when the structure deforms laterally to the right under lateral loading, the BRBs and perimeter columns on the right-hand side are in compression, and in tension on the left-hand side. The outrigger truss, BRBs, and perimeter columns act in series to provide resisting moments on the core structure at each outrigger elevation, so that the lateral deformation and base overturning moment of the core structure can be reduced. Once the BRBs yield, they start dissipating energy. The maximum force demands for the outrigger truss members and perimeter columns are limited by the maximum axial force capacity of the BRBs. When the viscous dampers are employed in damped-outrigger system, the velocity-dependent viscous dampers are more efficient in limiting the maximum acceleration and also applicable to control wind vibration. However, the high strength and stiffness of BRB make the BRB-outrigger system to be more suitable in controlling the maximum inter-story drift response and mitigating damages for non-structural elements of the building. In addition, the BRB-outrigger system can function as a conventional outrigger system during frequent small earthquakes through its high elastic stiffness of the BRBs, and it can dissipate energy during moderate to maximum considered earthquake through the BRBs' stable hysteretic behavior.

When BRB is adopted as the energy dissipation device in the damped-outrigger system, the dynamic characteristics of the overall

structure and the associated seismic demand are affected by both the outrigger elevation and the stiffness of the BRB. Therefore, the aims of this study are to propose a method to evaluate the seismic response of the multiple BRB-outrigger system with various outrigger elevations, investigate the optimal outrigger elevations in order to minimize the seismic response, and study the relationships between the flexural rigidity of the core structure, the axial stiffness of the perimeter columns, and the BRBs in the dual BRB-outrigger system. The dynamic characteristics are studied and the seismic response is evaluated using the spectral analysis (SA), incorporating the concept of equivalent damping ratio to include the inelastic responses of the BRBs. The SA results are then validated by performing a nonlinear response history analysis (NLRHA). The continuous seismic response distributions with various outrigger elevations are demonstrated. The maximum roof drift ratio ( $\theta_{max}$ ), inter-story drift ( $\gamma_{max}$ ), overturning moment at the core structure base ( $M_{c,max}$ ), and the additional axial force demand for the perimeter column ( $C_{1,max}$ ) are adopted as indicators for judging the optimal outrigger elevations. The comparisons of seismic performance between the single and the dual BRB-outrigger systems assist the design engineers to determine the outrigger elevation and number. This study concludes with a design recommendation and presents design charts for preliminary design purposes.

## 2. Analytical models

This study uses a simplified structure to perform the modal analysis and SA. The effectiveness of utilizing the simplified structure is verified by performing a NLRHA on a member-by-member (MBM) model using OpenSees [14].

### 2.1. Simplified structure

Fig. 2 shows the simplified structure of height  $h$  with BRB-outriggers on  $n$ -levels, where  $l_i$  is the outrigger truss span. The lateral flexural rigidity and mass of the building are assumed to be concentrated at the core structure. The core structure is modeled by a cantilever column, which is assumed to deform in linear elasticity. The bases of the perimeter columns are free to rotate. The two ends of each BRB are pin-connected to the perimeter column and outrigger truss ends. The ends of the outrigger truss close to the core structure have full moment transfer capacity. For the  $j$ th level of the BRB-outrigger,  $k_{ij}$  and  $k_{dj}$  are the flexural stiffness of outrigger truss and the BRB axial stiffness, respectively. The elevation of outrigger at the  $j$ th level ( $h_j$ ) is defined as follows:

$$h_j = \prod_{i=j}^n \alpha_i h \quad (1)$$

where  $\alpha_i$  is the elevation ratio of the  $i$ th layer to the  $(i + 1)$ th layer of BRB-outrigger, and  $\alpha_n$  is ratio of the  $n$ th layer BRB-outrigger elevation to the building height. As the BRB-outriggers apply resisting moments on the core structure, the structure can be simplified to a continuous cantilever column with rotational springs attached. As all the BRB-outriggers share the same perimeter column, the rotational springs are interdependent. Two types of analytical models were used in this study. The first type analytical model is discrete mass (DM) model. The DM model was constructed by following the simplified structure and was used to perform the SA and NLRHA using OpenSees for the parametric study. Fig. 3 shows the DM model with dual BRB-outrigger system. The BRBs are modeled using truss elements, while the others are modeled using beam column elements. The material properties for the BRB elements are bilinear with a post-yield stiffness ratio of 0.01, and the other members are linearly elastic. The length of each BRB is 1 m. The perimeter column bases are free to rotate. The mass is distributed evenly on the height of core structure with a spacing of 1 m. The second type of analytical model is the member-by-member (MBM) model. The

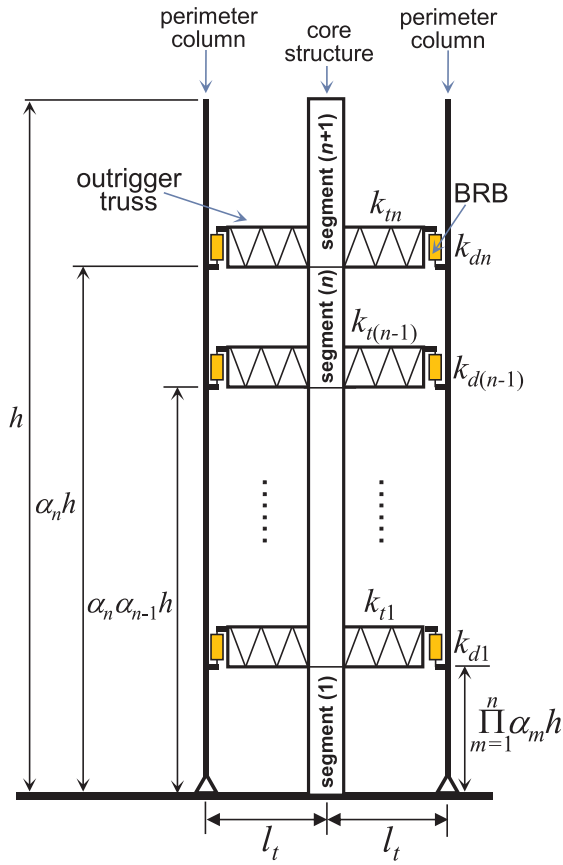


Fig. 2. Simplified structure.

MBM model includes all structural details such as the core structure and the floor beams, and considers the full BRB length as shown in Fig. 4. The core structure is represented by a braced frame, and the floor beams are modeled as truss elements. The purpose of using MBM model is to verify the effectiveness of using DM model to represent a real structure with BRB-outrigger.

2.2. Parameter definitions

This study focuses on investigating the seismic performance of dual BRB-outrigger systems. Dimensionless parameters are introduced based on dual BRB-outrigger systems. The outrigger stiffness parameter  $S_{bc2}$  is defined as the ratio of rotational stiffness provided by the upper BRB-outrigger, when the BRB axial stiffness is infinity, to the rotational stiffness of the core structure as follows:

$$S_{bc2} = \left( \frac{l_t^2}{1/k_t + \alpha_2/k_c} \right) / \left( \frac{EI}{h} \right) = \frac{l_t^2 h}{EI(1/k_{t2} + \alpha_2/k_c)} = \frac{l_t^2 h k_c}{EI(R_{dt2}/R_{d2c} + \alpha_2)} \tag{2}$$

where  $k_c$  and  $EI$  are the perimeter column axial stiffness with a length of  $h$  and the flexural rigidity of the core structure, respectively.  $R_{dt2}$  ( $=k_{d2}/k_{t2}$ ) and  $R_{d2c}$  ( $=k_{d2}/k_c$ ) are the BRB stiffness parameters. The value of  $S_{bc2}$  is used to indicate the magnitude of the outrigger effect on structure. The greater the value of  $S_{bc2}$ , the greater the outrigger effect. The outrigger effect can be enhanced by a longer outrigger truss span ( $l_t$ ), stiffer outrigger trusses, and stiffer perimeter columns (greater  $k_t$  and  $k_c$ ). In addition, for very tall buildings, the value of  $EI/h$  could significantly increase because of the higher seismic demand. Therefore, the outrigger truss member and perimeter column sizes should be increased in order to meet the desired outrigger stiffness parameter. The BRB parameter  $R_{d2c}$  ( $=k_{d2}/k_c$ ) is defined as the ratio of the BRB axial stiffness in the upper outrigger ( $k_{d2}$ ) to the perimeter column axial

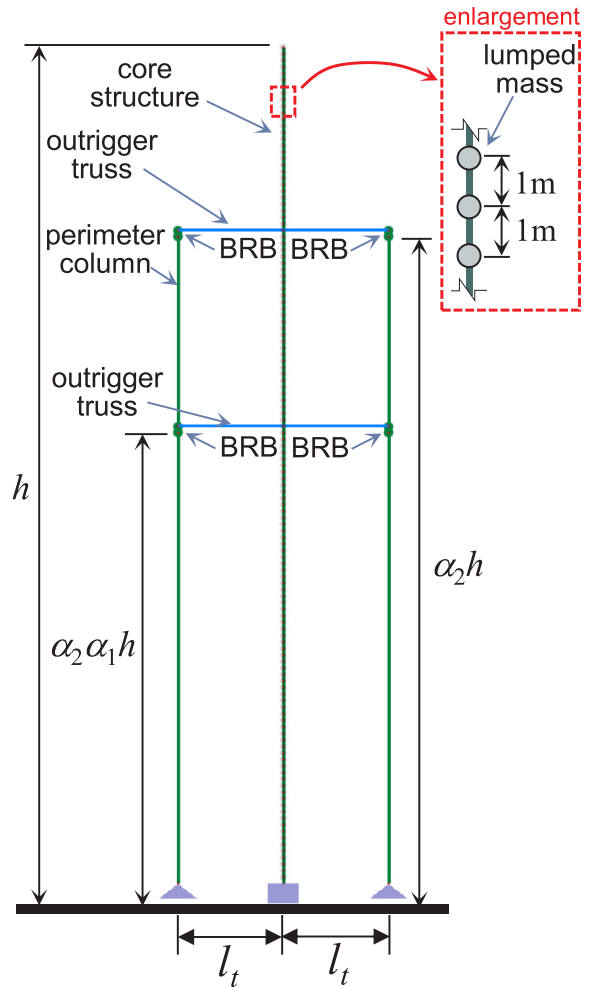


Fig. 3. DM model.

stiffness ( $k_c$ ). In design practices, the perimeter column sizes are primarily designed according to the gravity load requirements. Therefore,  $R_{d2c}$  can provide engineers with a quick estimation of the required BRB sizes. The second BRB parameter  $R_{kd}$  ( $=k_{d1}/k_{d2}$ ) is defined as the ratio of the axial stiffness of the BRB in the lower outrigger ( $k_{d1}$ ) to the axial stiffness of the BRB in the upper outrigger ( $k_{d2}$ ). When  $R_{kd}$  is greater than 1.0, the BRB in the lower outrigger is stiffer than the upper one, and vice versa. If  $R_{kd} = 0$ , it is a single BRB-outrigger system. The parameter  $R_{dtj}$  is used to describe the ratio of  $k_{dj}$  to  $k_{tj}$  for the  $j$ th level BRB-outrigger. In order to generate sufficient deformation demand on the BRBs, the  $R_{dtj}$  should be as small as possible. For simplicity, the values of  $R_{dt1}$  and  $R_{dt2}$  are set as 0.1 for the dual BRB-outrigger system in this study.

2.3. Spectral analysis

The SA procedure is a quicker alternative to the time-consuming NLRHA. It estimates the peak seismic response of a structure from the given response spectrum. For a multi-degree-of-freedom system, the peak response of each mode is obtained separately, and then combined together to obtain the overall response. Even though the SA may not accurately estimate the peak response of a structure subjected a particular earthquake, the results are considered to be accurate enough for practical design applications. In this study, the SA procedure, incorporating an equivalent damping ratio [15] in order to consider the effect of inelastic deformation of BRBs, is used to evaluate the seismic performance of the dual BRB-outrigger system. The response of each mode is calculated separately and then combined by using the square

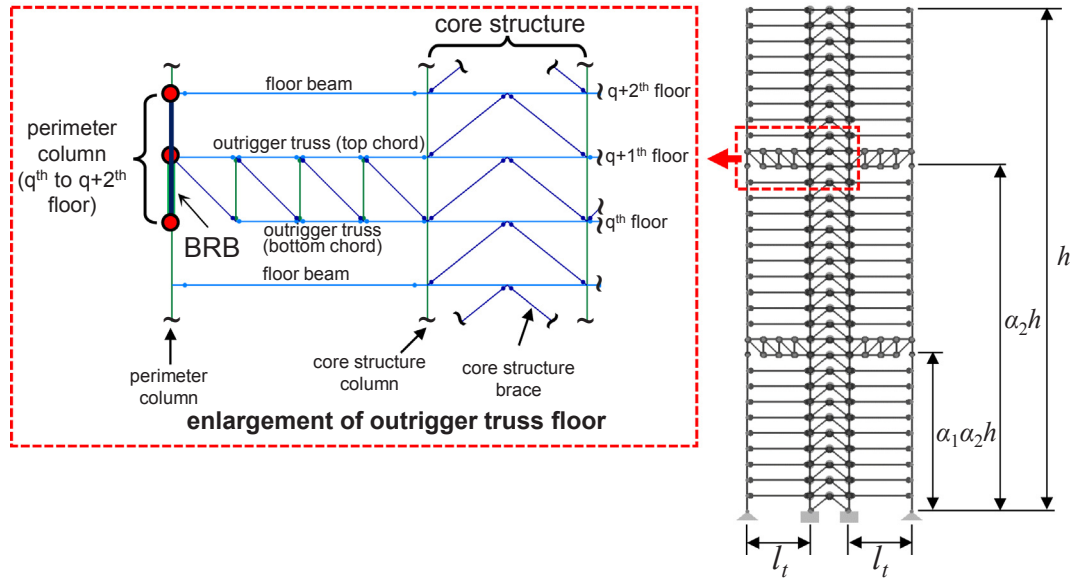


Fig. 4. Illustration of MBM model.

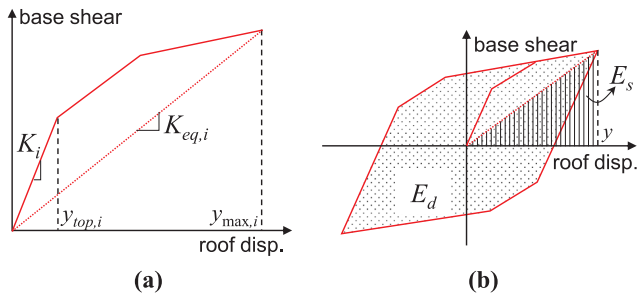


Fig. 5. Relationship (a) between base shear and roof displacement obtained from MPA, and (b) between  $E_d$  and  $E_s$ .

root of the sum of the squares (SRSS) method. It is anticipated that the yielding of the BRB only results in a marginal decrease in the BRB-outrigger system stiffness. Therefore, it is assumed that the modal superposition principle based on elastic mode shapes remains applicable when the BRBs deform inelastically [16]. The maximum roof drift ( $\theta_{max}$ ) and maximum inter-story drift ( $\gamma_{max}$ ) are calculated based on the SRSS superposed deformed shape. The BRBs in multiple BRB-outrigger systems would not yield simultaneously. Therefore, this study uses the DM model to perform a modal pushover analysis (MPA) [16] by using OpenSees to obtain the base shear and roof displacement relationship. Fig. 5a shows a MPA curve of the  $i$ th mode, where  $y_{top,i}$  is the roof displacement when the first BRB yields,  $K_i$  is elastic modal stiffness, and  $K_{eq,i}$  is the equivalent stiffness when the roof displacement reaches its maximum value of  $y_{max,i}$ . It should be noted that the lateral force pattern used in the MPA remains the same as the elastic mode shape even after the BRB yields. The equivalent damping ratio ( $h_{eq,i}$ ) of the  $i$ th mode response with a ductility of  $\mu_i$  is calculated as follows:

$$h_{eq,i} = h_0 + \frac{1}{y_{max,i}} \int_{y_{top,i}}^{y_{max,i}} \frac{E_d(y)}{4\pi E_s(y)} dy, \quad \mu_i = \frac{y_{max,i}}{y_{top,i}} \quad (3)$$

where  $E_d(y)$  and  $E_s(y)$  are the energy dissipated by the BRB-outrigger system per loop and the strain energy with a roof displacement of  $y$  (Fig. 5b), respectively, and  $h_0$  is the inherent damping ratio. The  $h_0$  is assumed to be 0.02 for each mode in this study. The response spectrum is reduced because of the increased damping ratio by using the reduction factor  $D_{h,i}$  expressed as follows [17]:

$$D_{h,i} = \sqrt{\frac{1 + \kappa h_0}{1 + \kappa h_{eq,i}}}, \quad \begin{matrix} \kappa = 25 \text{ for observed ground motions} \\ \kappa = 75 \text{ for artificial ground motions} \end{matrix} \quad (4)$$

The maximum roof displacement ( $y'_{max,i}$ ) can be estimated as follows:

$$y'_{max,i} = D_{h,i} S_d(T_{eq,i}, h_0) \Gamma_i \phi_i(h) \quad (5)$$

where  $T_{eq,i}$  is the equivalent vibration period,  $\Gamma_i$  is the  $i$ th modal participation factor, and  $\phi_i(h)$  is the roof displacement in the  $i$ th mode shape.  $S_d(T, h_d)$  is the spectral displacement at period  $T$  and damping ratio  $h_d$ . In this study, the spectral displacement is calculated based on the design acceleration spectrum as shown in Fig. 6. After the first computation, replace the  $y_{max,i}$  in Eq. (3) with  $y'_{max,i}$  if they differ significantly. The calculation of the maximum roof displacement is an iterative procedure, and it should be continued until the  $y_{max,i}$  used in computing  $h_{eq,i}$  (Eq. (3)) is sufficiently close to the  $y'_{max,i}$  obtained from Eq. (5). In this study, the iteration is performed until the difference between  $y_{max,i}$  and  $y'_{max,i}$  become smaller than 5%. The response of the first four modes are calculated separately, and then combined using the SRSS method. The effective modal mass ratio of the  $i$ th mode ( $m_{eff,i}$ ) is used to judge the participation of the  $i$ th mode, and a higher  $m_{eff,i}$  suggests a greater contribution from the  $i$ th mode in the seismic response. The  $m_{eff,i}$  is calculated as follows:

$$m_{eff,i} = M_i \Gamma_i^2 / \sum_{j=1}^4 M_j \Gamma_j^2 \quad (6)$$

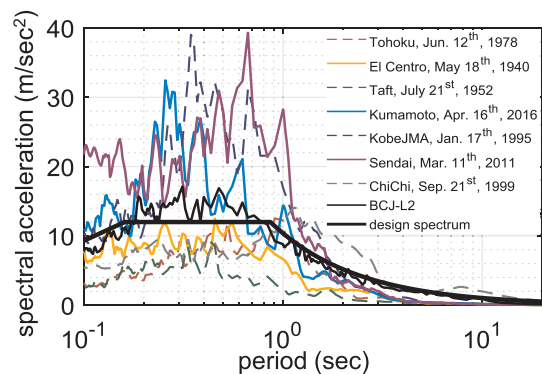


Fig. 6. Response spectra of ground motions adopted in NLRHA.

where  $M_i$  is the generalized mass for the  $i$ th mode. If  $\psi(x)$  is the SRSS combined deformed shape, the  $\theta_{\max}$  and  $\gamma_{\max}$  are calculated as follows:

$$\theta_{\max} = \frac{|\psi(h)|}{h}, \quad \gamma_{\max} = \max \left[ \left| \frac{d}{dx} \psi(x) \right|, 0 \leq x \leq h \right] \quad (7)$$

### 2.4. Nonlinear response history analysis

The NLRHA can precisely estimate the seismic response of a structure under a particular earthquake, as the nonlinear behavior and the response of all modes are included. However, the NLRHA is time consuming and dependent on the selected input ground motion. Thus, the NLRHA results are usually used to confirm seismic performance of a structure. In this study, the NLRHA was performed using eight (seven observed and one artificial) ground motions. Fig. 6 shows the acceleration spectra of the eight original observed ground motions (scale factors equal to 1). Except the ChiChi ground motion, the other observed ground motions are commonly used in NLRHA in Japan. The artificial ground motion BCJ-L2 was generated based on past seismic history to match a Japanese seismic intensity of 6-upper (peak ground motion of 315–400 Gal) [18]. The spectral accelerations of the ground motions are scaled so that the mean of the spectral accelerations fit the design spectral acceleration within the range of  $0.2T_1$  to  $1.5T_1$ , where  $T_1$  is the 1st mode period. Therefore, the SA and NLRHA results are comparable. Fig. 7 demonstrates the acceleration spectra of the scaled ground motion used for a 16-story model (which will be introduced later) with  $T_1 = 1.031$  s. A Rayleigh damping ratio of 0.02 for the 1st and 2nd modes was applied for all NLRHA. The average of the NLRHA results obtained from the eight ground motions are used to verify the SA results. In this study, unless otherwise stated, the NLRHA refers to the analysis results calculated from the average of using eight scaled ground motions.

## 3. 96-Story model

A 96-story model is used to demonstrate the seismic performance of the BRB-outrigger system by using SA and NLRHA procedures. The effectiveness of using the DM model to represent the MBM models is also investigated.

### 3.1. Analytical model

Fig. 8a shows the BRB-outrigger floor framing plan at the outrigger floor. The core structure and two elevations of the outrigger are responsible for resisting lateral loads in the EW direction. In the engineering design practices, it is preferable to design the core structure to

deform elastically. For simplicity, only one outrigger frame elevation and half of the core structure are considered in the analytical model. The building is 384 m tall, and each story is 4 m high. The two BRB-outriggers are located at elevations of 268 m ( $\alpha_2 = 0.7$ ) and 132 m ( $\alpha_1 = 0.5$ ). The dead load (which is the mass source) and live load are  $0.8 \text{ tonf/m}^2$  and  $0.3 \text{ tonf/m}^2$ , respectively. The core structure flexural rigidity ( $EI$ ) is  $2.2 \times 10^{11} \text{ kN}\cdot\text{m}^2$ . The perimeter column is designed according to the gravity load demands at the 1st story, and the size is box  $2200 \times 2200 \times 100 \text{ mm}$  (SN490 steel grade) with infill concrete with a compressive strength of 10,000 psi (70 MPa). Because the infill concrete is not able to develop tensile strength, the calculation of  $k_c$  ( $437,500 \text{ kN/m}$ ) is based on the steel box only. Table 1 presents the design details of the BRB in the lower (BRB<sub>1</sub>) and upper (BRB<sub>2</sub>) outriggers. The calculation of the BRB yield deformation ( $u_{d,y}$ ) will be discussed in detail in the next section. As the required BRB yield deformations are greater than 10 mm, the BRB length should be approximately between 6 m and 10 m. Therefore, the 8 m long BRBs are arranged vertically, spanning two stories as shown in Fig. 8b. The upper end of the BRB connects to the left end of the top chord of the outrigger truss, and the lower end connects to a bracket that is fixed to the perimeter column. The two ends of the BRB are designed with pinned connection detail, and the floor beam ends are designed with shear connection detail. The parameters  $S_{bc2}$ ,  $R_{d2c}$ , and  $R_{kd}$  are 0.26, 2.02, and 0.97, respectively, and  $R_{dt1}$  and  $R_{dt2}$  are set as 0.1. Table 2 summaries the key parameters used in the DM and the MBM models. The modulus of elasticity are 200 GPa for the BRB material properties in both the DM and the MBM models. As the BRB element lengths are 1 m and 4 m in the DM and the MBM models, respectively, the different values of the cross-sectional area and the material yield stress for the BRB elements as shown in Table 2 are used in the DM and the MBM models, so that the axial stiffness and strength match with the BRB design shown in Table 1. For simplicity, the gravity loads and secondary effect have been excluded in the analytical models. Furthermore, in order to compare the seismic performances between single and dual outrigger systems, and between conventional elastic outrigger and BRB-outrigger systems, five models are analyzed. The model without any outrigger (Core) is used as a benchmark model. The models with single (Single) or dual (Dual) BRB-outrigger are used to compare the models with single (SingleElastic) or dual (DualElastic) conventional elastic outrigger systems. In the SingleElastic and DualElastic models, the BRB yield deformation ( $u_{d,y}$ ) is set at infinity. For the Single and SingleElastic models, there is only an upper outrigger.

### 3.2. Analysis results

Table 3 presents the modal analysis results of the DM and MBM models. When the Core model is compared with the Single and Dual models, the reduced vibration periods indicate that the BRB-outrigger provides additional stiffness to the structure. This effect is more significant in the Dual model than in the Single model. As can be seen in Table 3, the vibration periods of the MBM models are slightly longer than the DM models. This is because of the different mass distributions in the DM (1 m mass spacing), and MBM (4 m mass spacing) models. However, the marginal differences in the modal analysis results between different models suggest that the DM model could be a good representation of the MBM model. Figs. 9 and 10 show the roof drift histories and the relationship between the BRB normalized axial force and core strain obtained from NLRHA using BCJ-L2 as the input ground motion. The BRB responses and roof drift peaks obtained from the DM and MBM models are in close approximation. This suggests that the DM model can be used in both the SA and NLRHA for the parametric study.

Table 4 and Fig. 11 show the SA results and the MPA curves of the Dual model when the roof displacement reaches  $y'_{\max,i}$  (Eq. (5)). The MPA curves indicate that the BRB<sub>1</sub> and BRB<sub>2</sub> yield almost simultaneously for the 1st and 2nd mode responses. The 1st and 2nd modal stiffness decrease by approximately 18% and 21%, respectively, after

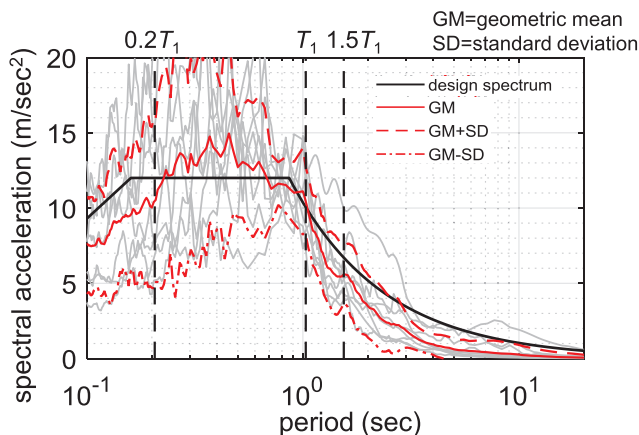


Fig. 7. Acceleration spectra of the scaled ground motions used in NLRHA for the 16-story model.

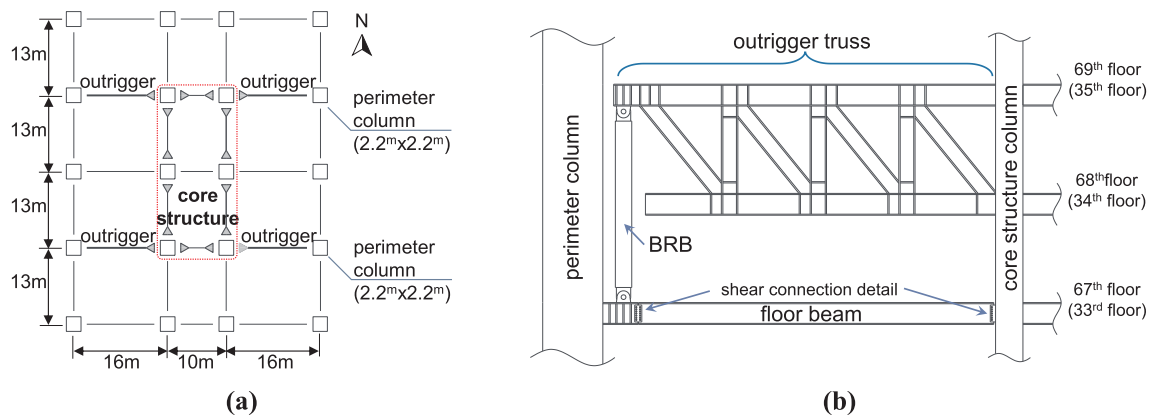


Fig. 8. (a) Outrigger floor framing plan of 96-story model, and (b) enlargement of BRB-outrigger detail.

Table 1  
BRB design of 96-story model.

Member	Material	Material yield stress (MPa)	Cross-sectional area (mm <sup>2</sup> )			Segment length (mm)			$k_d$ (kN/m)	$u_{d,y}$ (mm)
			Core	Transition	Joint	Core	Transition	Joint		
BRB <sub>2</sub>	SN490	325	33,831	43,281	52,731	7000	75	425	883,017	12.5
BRB <sub>1</sub>			28,575	40,815	53,055	5000	136	1364	858,146	10.8

BRB<sub>1</sub> and BRB<sub>2</sub> yield. The  $E_d/E_s$  presented in Table 4 is the ratio of the energy dissipated by the BRBs to the total strain energy of the system, and  $h_{eq,i}$  is the equivalent damping ratio of the  $i$ th mode response as obtained from Eq. (3). The 1st mode response dominates the overall response, as it has the greatest contribution to  $\theta_{max}$ . The maximum axial deformations of BRB<sub>1</sub> and BRB<sub>2</sub> and the ductility ( $\mu_i$ ) indicate that both the 1st and 2nd mode responses are inelastic. However, the values of  $E_d/E_s$  indicate that the energy dissipation mechanism is essentially governed by the 1st mode response. Based on the analysis results, the SA procedure considering the responses of the first four modes should be adequate. Fig. 12 shows the maximum lateral displacement and inter-story drift distributions along the building height as obtained from the SA and NLRHA with BCJ-L2 ground motion. The NLRHA results obtained from the DM and MBM models are in good agreement. Differences between the SA and NLRHA results are because the SA calculation is based on the modal superposition using elastic mode shapes. Although the NLRHA results are dependent on ground motion, the peak responses and trends are similar in the SA and NLRHA results. Table 5 presents the peak response from SA and NLRHA. The SA well estimates the maximum roof drift ( $\theta_{max}$ ) responses. The maximum roof acceleration ( $a_{max}$ ) response calculated from the SA show that the SingleElastic and the DualElastic models develop larger  $a_{max}$  than the Single and the Dual models, respectively. This effect can also be observed from the NLRHA results but is less obvious. The maximum base shear ( $V_{c,max}$ ) and the maximum core structure base overturning moment ( $M_{c,max}$ ) calculated from NLRHA suggest that the outrigger system can effectively reduce the  $V_{c,max}$  and  $M_{c,max}$  responses, and the Single and Dual models with energy dissipation mechanism developed by BRB-outrigger perform better. The  $E_d/E_s$  values for BRB<sub>1</sub> and BRB<sub>2</sub>, and the corresponding equivalent damping ratios ( $h_{eq}$ ) are also presented in Table 5.

Table 2  
Key parameters used in the 96-story DM and MBM models.

Model	Mass	Core structure	BRB element length		BRB element cross-sectional area (mm <sup>2</sup> )		BRB element material yield stress (MPa)	
			BRB <sub>2</sub>	BRB <sub>1</sub>	BRB <sub>2</sub>	BRB <sub>1</sub>	BRB <sub>2</sub>	BRB <sub>1</sub>
DM	225 ton at each mass node	Cantilever column	1 m		4415	4291	2500	2160
MBM	900 ton at each floor	10 m-span braced frame	8 m		35,321	34,326	313	270

The values of  $E_d/E_s$  obtained from the NLRHA results are calculated from the ratio of the energy dissipated by BRBs to the total seismic input energy. The  $E_d/E_s$  values are zero because the BRBs deform elastically in the SingleElastic and DualElastic models. The  $h_{eq}$  estimated by the SA are only slightly smaller than the NLRHA results. This suggests that the SA procedure using equivalent damping ratio could properly evaluate the energy dissipation performance of BRBs. Based on the analysis results, the deformation-related seismic performance indicators ( $\theta_{max}$  and  $\gamma_{max}$ ) calculated from the SA and NLRHA, the overturning moment at core structure base ( $M_{c,max}$ ), and the maximum perimeter column axial force ( $C_{1,max}$ ) obtained from the NLRHA results were adopted as seismic performance indicators.

Table 6 presents the seismic response reductions compared with the Core model. The value of  $\theta_{max}$  can be reduced by approximately 10% with the SingleElastic and DualElastic models. If the BRB-outrigger system is applied, the reduction can be increased to approximately 12% and 18% for the Single and Dual models, respectively. The conventional outrigger models (SingleElastic and DualElastic) reduce  $\theta_{max}$  by increasing the system stiffness, while they may not be able to effectively reduce acceleration responses due to the increased stiffness and elastic response. In addition, because of the hysteretic responses of the BRBs, the Single and Dual models perform better in mitigating the roof drift after the peak responses than the SingleElastic and DualElastic models, as shown in Fig. 9. In the 96-story model, the maximum inter-story drift ( $\gamma_{max}$ ) occurs at the top story of the building, and  $\gamma_{max}$  is reduced by approximately 10% to 20% by the outrigger system, if compared with the Core model. However, the NLRHA results indicate that the BRB-outrigger system does not exhibit better reductions in  $\gamma_{max}$  than the conventional elastic outrigger system. This could be because the location where  $\gamma_{max}$  develops is higher than the upper BRB-outrigger. In

**Table 3**  
Modal analysis results of 96-story models.

Model	Mode	Period (sec)				Effective modal mass ratio (%)			
		1st	2nd	3rd	4th	1st	2nd	3rd	4th
DM	Core	8.449	1.348	0.481	0.246	68.2	21.0	7.2	3.6
	Single	7.804	1.329	0.481	0.245	69.0	20.1	7.2	3.7
	Dual	7.631	1.313	0.481	0.244	68.7	20.6	7.1	3.6
MBM	Core	8.485	1.361	0.486	0.248	68.3	21.0	7.2	3.5
	Single	7.835	1.341	0.486	0.248	69.0	20.1	7.2	3.7
	Dual	7.658	1.325	0.485	0.246	68.7	20.6	7.1	3.6

addition, the conventional outrigger provides greater rotational spring stiffness, which could be more effective in reducing inter-story drift responses. As shown in Fig. 12b, the lower outrigger effectively reduces the inter-story drift at elevations close to the lower outrigger. Furthermore, the Dual model exhibits better inter-story drift reductions at elevations close to the lower outrigger than the DualElastic model. The conventional elastic outrigger system (SingleElastic and DualElastic models) exhibits a 6% to 8% decrease in the maximum base shear ( $V_{c,max}$ ), whereas the BRB-outrigger system (Single and Dual models) reduces the  $V_{c,max}$  by approximately 10%. This is because the conventional outrigger, that keeps the response elastic, could generate greater lateral force demands during an earthquake. However, the stiffness of the BRB-outrigger system decreases after the BRB yields. In addition, the energy dissipated by BRBs also assists in reducing  $V_{c,max}$ . For the maximum overturning moment at the core structure base ( $M_{c,max}$ ), the reductions are approximately 10% for the SingleElastic and Single models, and approximately 10% and 13% for the DualElastic and Dual models, respectively. If compared with the single outrigger, the additional lower outrigger in the dual outrigger system applies an additional reaction moment close to the core structure base. Therefore, the  $M_{c,max}$  can be further reduced if compared to the single outrigger system. Table 5 also presents the maximum perimeter column axial force at the base ( $C_{1,max}$ ) and in between the two outriggers ( $C_{34,max}$ ), where the subscripts 1 and 34 refer to the perimeter column in the 1st and 34th stories, respectively. The perimeter column axial forces of the BRB-outrigger (Single and Dual) models are approximately only 20% of those of the conventional outrigger systems (SingleElastic and DualElastic models). This indicates that the yielding of BRBs effectively limits the maximum force developed in the perimeter columns and outrigger truss members. If the dual outrigger system is compared to the single outrigger system,  $C_{1,max}$  in the dual outrigger system is greater than that in the single outrigger system, but  $C_{34,max}$  in the dual outrigger system is slightly smaller than that in the single outrigger system. This is because the lower BRB-outrigger applies an additional reaction moment on the core structure, and thus generates additional axial force demands on the perimeter columns. Compared to the conventional outrigger system, the BRB-outrigger system can achieve better performance by reducing the seismic response without excessively increasing the perimeter column axial forces. In addition, the dual BRB-outrigger system performs better in reducing the overall seismic response by approximately 3% to 7% than the single BRB-outrigger system. Based on the

analysis results, the SA and NLRHA exhibit similar trends in the reduction of the seismic response, and the differences between the SA and NLRHA results should not affect the aim of parametric study on the optimal design. The DM model is used for investigating the optimal outrigger elevations and optimal values of  $R_{d2c}$  and  $R_{kd}$  in the following sections.

#### 4. Analysis procedure of parametric study

Table 7 shows the analytical models used in this study. The 16-story, 32-story, 64-story, and 96-story models have heights of 64 m, 128 m, 256 m, and 384 m, respectively. The additional three models (16-storyB, 16-storyC, and 32-storyD) are included to investigate the relationship between  $S_{bc}$  and  $R_{d2c}$  in order to create a more uniform distribution of the  $S_{bc}$  values (which will presented later in this section). The structural plan and the mass source are the same as the 96-story example, as shown in Fig. 8a, but the  $l_i$  is 14.5 m, 12.8 m, and 13.8 m for the 16-storyB, 16-storyC, and 32-storyD models, respectively. The magnitude of the outrigger effect is indicated by  $S_{bc2}$  value when  $\alpha_2$  is 0.7. The outrigger effect is set smaller for taller building, because of the longer perimeter columns providing smaller values of  $k_c$  and greater values of  $EI$  because of higher seismic demand for taller buildings. The values of  $EI$  are selected so that the fundamental vibration period of the core structure is within a realistic range (for example  $0.03h$ ). The value of  $R_{d2c}$  ranges from 0.1 to 3, and the value of  $R_{kd}$  is set as either 0 (single BRB-outrigger case), 0.5, 1, or 3. In each analysis set, with the selected  $R_{d2c}$  and  $R_{kd}$  values, the  $\alpha_1$  and  $\alpha_2$  vary from 0 to 1, and the value of  $k_c$  can be calculated using Eq. (2). The value of  $R_{dt}$  is set as 0.1 in every analysis in the parametric study.

The BRB yield deformation ( $u_{d,y}$ ) is critical as it determines when the BRBs start yielding and dissipating energy. If  $u_{d,y}$  is too large, the BRB could only slightly yield, or even remain elastic, during an earthquake, which would result in a low energy dissipation efficiency. However, if  $u_{d,y}$  is too small, the BRB could easily yield even during a small earthquake, or fracture due to low-cycle fatigue before the end in a moderate earthquake. In this study, the BRB yield deformations are determined as follows. The first step is to calculate the spectral lateral deformed shapes of the first four modes of the structure based on the design spectrum. The second step is to combine the spectral deformed shapes of the first four modes using SRSS method. The combined deformed shape is then scaled until the roof drift reaches  $\theta_r$ , which is the

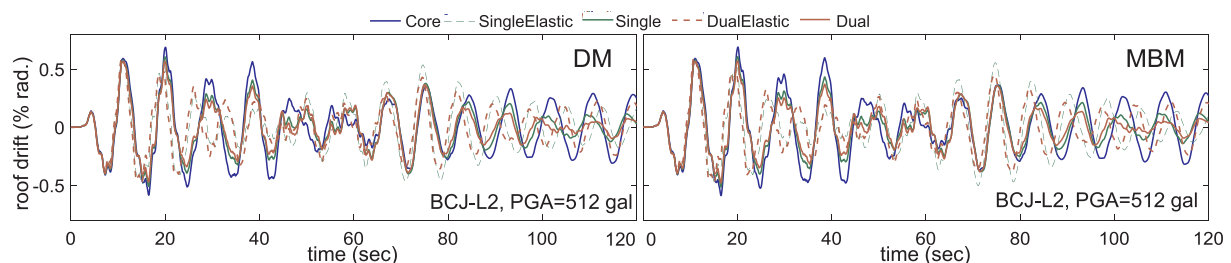


Fig. 9. Roof drift history obtained from NLRHA using DM and MBM models.

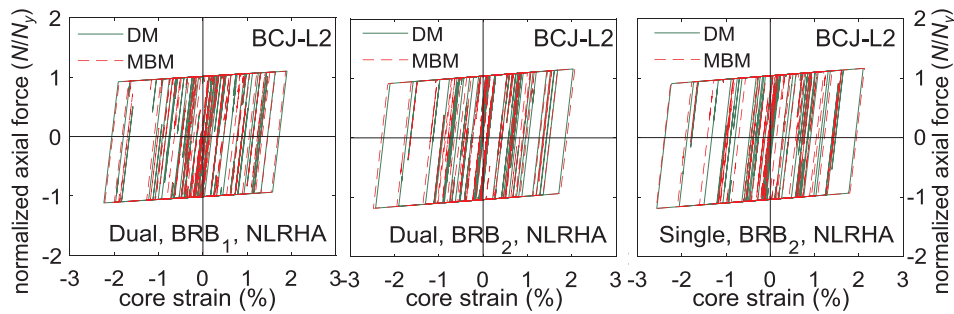


Fig. 10. Relationships between BRB normalized axial force and core strain from NLRHA using BCJ-L2 ground motion.

Table 4  
SA results of Dual model of 96-story models.

Mode	$\theta_{max,i}$ (% rad.)	$y_{top,i}/h$ (% rad.)	$\mu_i$	Maximum BRB axial deformation (mm)		$E_d/E_s$	$h_{eq,i}$
				BRB <sub>1</sub>	BRB <sub>2</sub>		
1st	0.707	0.184	3.83	103	143	0.23	0.038
2nd	0.074	0.044	1.68	-17	26	0.09	0.027
3rd	0.009	0.045	0.20	-2.0	0.8	0	0.020
4th	0.002	0.011	0.18	1.7	-1.2	0	0.020

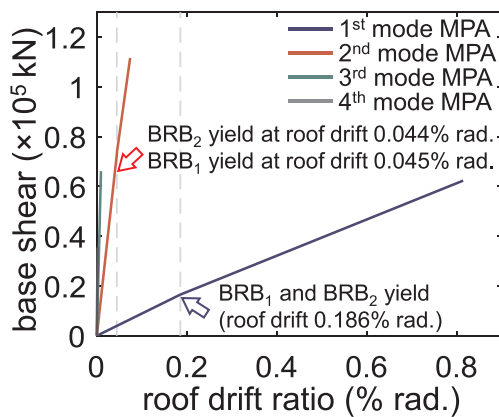


Fig. 11. MPA curves for Dual model.

maximum allowable elastic roof drift limit, for example 1/750 or 1/550. The axial deformations of the BRBs under this combined deformed shape with the roof drift ratio of  $\theta_r$  are adopted as the yield deformations. As the BRBs are deformation-dependent energy dissipation

devices, it is believed that this combined deformed shape should best represent the deformed shape right before the two BRBs yield. The yield deformations of the aforementioned 96-story model BRBs are calculated when  $\theta_r$  equals 1/550. As the 1st mode dominates the overall response, BRB<sub>1</sub> and BRB<sub>2</sub> yield approximately simultaneously under the 1st mode MPA, as shown in Fig. 11. In the 2nd mode MPA, the BRB<sub>1</sub> yields immediately after BRB<sub>2</sub> yields. The BRBs yielding simultaneously is desirable as it ensures that the BRBs start dissipating energy together, and the deformation concentration at weak stories, or at certain BRB-out-rigger levels, could be avoided.

The 16-story and the 96-story models are used to investigate the effects of higher mode contribution on the peak response by performing SA. Both the 16-story and the 96-story models have the same parameters of  $\alpha_2 = 0.7$ ,  $\alpha_1 = 0.5$ ,  $R_{d2c} = 1.0$ ,  $R_{kd} = 1.0$ , and  $\theta_r = 1/750$ . Table 8 shows the modal analysis and the SA results for the first four modes. The greater values of the effective modal mass ratios of the 2nd and 3rd modes in the 96-story model indicate that the participations from the 2nd and 3rd mode response are more significant in the 96-story model than in the 16-story model. In the 16-story model, the inelastic response only occurs in the 1st mode ( $\mu_1 > 1$ ). However, in the 96-story model, both the 1st and 2nd mode response is inelastic (both  $\mu_1$  and  $\mu_2$  are greater than 1) and thus contribute additional damping (both  $h_{eq,1}$  and  $h_{eq,2}$  are greater than 1). Fig. 13 shows the lateral displacement and the inter-story drift distribution along building height of the first four modes for the 16-story and 96-story models. In the lateral displacement responses, the contributions from the 2nd mode response in the 96-story model is slightly higher than the 16-story model. In addition, the influence from the 2nd mode response on inter-story drift responses is more significant than on the lateral displacement response for both the 16-story and 96-story models. This phenomenon is less obvious in the 16-story model. This could be due to the greater 2nd mode effective modal mass ratio and the inelastic 2nd mode response of the 96-story model. Based on the analysis results shown in Table 8 and

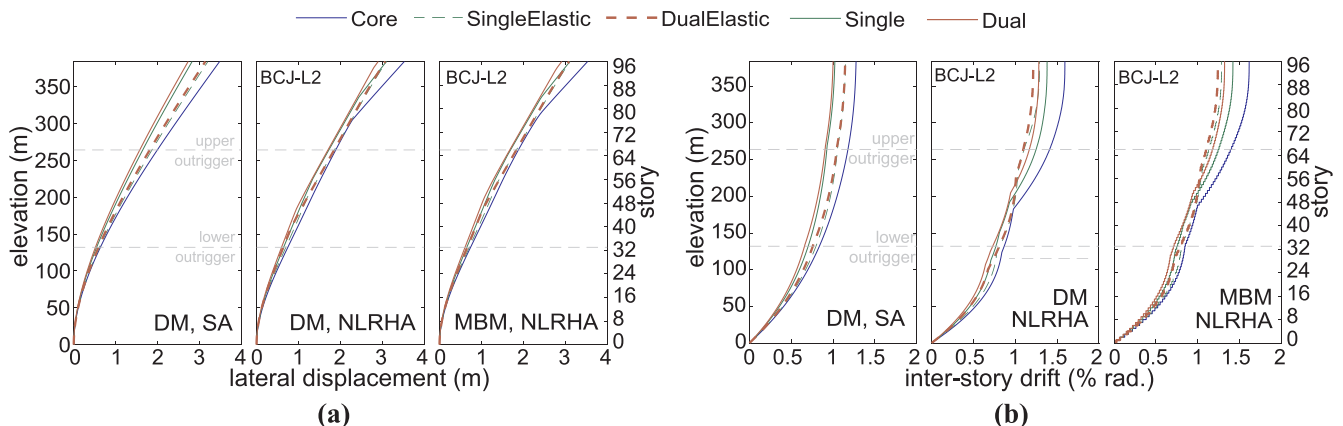


Fig. 12. (a) Lateral displacement and (b) inter-story drift distributions calculated from SA and NLRHA with BCJ-L2 ground motion.

**Table 5**  
Maximum responses from SA and NLRHA results.

		DM					MBM				
		Core	Single Elastic	Dual Elastic	Single	Dual	Core	Single Elastic	Dual Elastic	Single	Dual
$\theta_{max}$ (% rad.)	S	0.907	0.834	0.818	0.736	0.711	–	–	–	–	–
	A	0.935	0.809	0.815	0.810	0.772	0.935	0.803	0.803	0.807	0.768
$\gamma_{max}$ (% rad.)	S	1.27	1.15	1.14	1.02	1.00	–	–	–	–	–
	N	2.05	1.79	1.79	1.79	1.73	2.06	1.78	1.79	1.80	1.73
$a_{max}$ (m/sec <sup>2</sup> )	S	10.1	10.2	10.3	9.73	9.59	–	–	–	–	–
	N	13.4	12.5	12.7	12.5	12.3	18.0	17.4	16.7	17.7	16.4
$V_{c,max}$ ( $\times 10^5$ kN)	N	5.42	4.97	4.99	4.90	4.76	5.28	4.91	4.98	4.81	4.70
$M_{c,max}$ ( $\times 10^7$ kN -m)	N	4.39	3.98	4.01	3.93	3.80	4.32	3.93	4.00	3.88	3.77
$E_{d2}/E_s$ (%)	N	0	0	0	28.7	27.8	0	0	0	28.5	27.5
$E_{d1}/E_s$ (%)	N	0	0	0	0	15.2	0	0	0	0	15.2
$h_{eq}$	S	0.02	0.02	0.02	0.039	0.045	–	–	–	–	–
	N	0.02	0.02	0.02	0.043	0.054	0.02	0.02	0.02	0.043	0.054
$C_{34,max}$ ( $\times 10^4$ kN kN)	N	–	7.97	8.32	1.28	1.27	–	7.99	8.38	1.28	1.27
$C_{1,max}$ ( $\times 10^4$ kN kN)	N	–	7.97	8.01	1.28	2.09	–	7.99	8.02	1.28	2.10

S = SA, N = NLRHA.

Fig. 13, the responses obtained considering the first four modes is considered to be sufficient to incorporate the effects from the modes higher than the 1st mode.

**5. Analysis results**

As the BRB-outriggers increase the system stiffness to reduce the seismic response by applying resisting moments on the core structure, the outriggers at the elevations that result in greatest drop of vibration period indicates that the outrigger effect is the greatest. It is anticipated that the optimal outrigger elevations in minimizing seismic responses are also the outrigger elevations that have the greatest outrigger effect. Fig. 14 shows the 1st and 2nd mode vibration period distributions with respect to  $\alpha_1$  and  $\alpha_2$  for the 64-story model when  $R_{d2c}$  equals to 1 and 3 and  $R_{kd}$  equals to 1 and 3. The 1st mode vibration period distributions indicate that when  $\alpha_2$  is approximately 0.7 to 0.8, and when  $\alpha_1$  is approximately 0.6 to 0.7, the vibration periods are smallest. The 2nd mode vibration periods are the smallest when  $\alpha_2$  is around 0.8 to 0.9 and when  $\alpha_1$  is around 0.2 to 0.3. In addition, increasing  $R_{d2c}$  and  $R_{kd}$  stiffens the system, and causes the vibration period to decrease. Fig. 15 shows the yield deformations of BRB<sub>1</sub> ( $u_{d,y1}$ ) and BRB<sub>2</sub> ( $u_{d,y2}$ ) of a 64-story model with  $\theta_r = 1/750$  when  $R_{d2c} = 1$  and 3 and  $R_{kd} = 1$  and 3. The  $u_{d,y2}$  is maximum when  $\alpha_2$  is approximately 0.5 to 0.6 and  $\alpha_1$  is 0. The  $u_{d,y1}$  is maximum when  $\alpha_1$  is approximately 0.5 and when  $\alpha_2$  is 1. As the lower BRB-outrigger is closer to the upper BRB-outrigger,  $u_{d,y2}$  decreases and  $u_{d,y1}$  increases. In addition, a stiffer BRB (greater  $R_{d2c}$  or  $R_{kd}$  values) results in a smaller yield deformation. The differences between  $u_{d,y2}$  and  $u_{d,y1}$  would be greater if  $R_{kd}$  is greater than 1 (when  $k_{d1}$  is greater than  $k_{d2}$ ). The outrigger elevations that create the largest  $u_{d,y2}$  or  $u_{d,y1}$  could be also the optimal outrigger elevation, as they are in the most efficient configuration in generating the maximum deformation demand for the BRBs under the same  $\theta_r$ . Based on the vibration period

**Table 6**  
Differences of maximum responses compared to Core model.

		DM				MBM			
		SingleElastic	DualElastic	Single	Dual	SingleElastic	DualElastic	Single	Dual
$\theta_{max}$ (%)	SA	–8	–10	–19	–22	–	–	–	–
	NLRHA	–13	–13	–13	–17	–14	–14	–14	–18
$\gamma_{max}$ (%)	SA	–9	–10	–20	–21	–	–	–	–
	NLRHA	–13	–13	–13	–16	–14	–13	–13	–16
$a_{max}$ (%)	SA	1	2	–4	–5	–	–	–	–
	NLRHA	–7	–5	–7	–8	–3	–7	–2	–9
$V_{c,max}$ (%)	NLRHA	–8	–8	–10	–12	–7	–6	–9	–11
$M_{c,max}$ (%)	NLRHA	–9	–9	–10	–13	–9	–7	–10	–13

**Table 7**  
Parameters of analytical models.

Model	$h$ (m)	$l_i$ (m)	$EI$ (kN-m <sup>2</sup> )	$S_{be2}$ when $\alpha_2 = 0.7$	Fundamental period of core structure (sec)	$R_{d2c}$	$R_{kd}$
16-story	64	16	$4.1 \times 10^9$	3.03	1.74	0.1,	0,
32-story	128	16	$1.6 \times 10^{10}$	1.38	3.50	0.5,	0.5,
64-story	256	16	$6.5 \times 10^{10}$	0.66	6.92	1,	1, 3
96-story	384	16	$2.2 \times 10^{11}$	0.30	9.76	1.5,	
16-storyB	64	14.5	$4.1 \times 10^9$	2.48	1.74	2,	
16-storyC	64	12.8	$4.1 \times 10^9$	1.93	1.74	2.5,	
32-storyD	128	13.8	$1.6 \times 10^{10}$	1.02	3.50	3	

and yield deformation distributions, the optimal upper and lower outrigger elevations should be approximately 0.6 to 0.8 and 0.5 to 0.6, respectively.

Fig. 16a and 16b show the analysis results of  $\theta_{max}$ ,  $\gamma_{max}$ , maximum perimeter column axial force ( $C_{1,max}$ ), and maximum overturning moment at the core structure base ( $M_{c,max}$ ) of the 16-story model when  $\alpha_1$  and  $\alpha_2$  vary from 0 to 1,  $R_{d2c}$  is 0.1, 1, and 3, and  $R_{kd}$  is 1 and 3. The results of the single BRB-outrigger cases can be identified from Fig. 16 when  $\alpha_1$  is 0. The SA well estimates the results of  $\theta_{max}$  if compared with the NLRHA results. The trends of  $\theta_{max}$ ,  $\gamma_{max}$ , and  $M_{c,max}$  with respect to the outrigger elevations are similar. The values of  $\theta_{max}$ ,  $\gamma_{max}$ , and  $M_{c,max}$  primarily change with  $\alpha_2$ , and the changes in  $\alpha_1$  only marginally affect the responses. It appears that the upper BRB-outrigger dominates the overall response, and the presence of the lower BRB-outrigger assists in further enhancing the performance. The values of  $\theta_{max}$ ,  $\gamma_{max}$ , and  $M_{c,max}$  are minimum when  $\alpha_2$  and  $\alpha_1$  are approximately 0.7 and 0.6, respectively, and decrease with increasing  $R_{d2c}$ . This suggests that a greater value of  $R_{d2c}$  (stiffer BRB) provides a greater outrigger effect in

**Table 8**  
SA results of Dual model of the 16-story and 96-story models.

Mode	Vibration period (sec)		Effective modal mass ratio (%)		$\theta_{\max,i}$ (% rad.)		$\mu_i$		$h_{eq,i}$	
	16-story	96-story	16-story	96-story	16-story	96-story	16-story	96-story	16-story	96-story
1st	1.031	7.528	71.4	68.7	0.485	0.685	3.68	5.29	0.11	0.042
2nd	0.240	1.308	18.8	20.7	0.024	0.069	0.60	2.20	0.02	0.035
3rd	0.098	0.481	6.3	7.0	0.002	0.009	0.04	0.26	0.02	0.02
4th	0.048	0.244	3.5	3.6	0.001	0.002	0.09	0.19	0.02	0.02

mitigating the seismic response. However, as can be seen in Fig. 16, the decrease in seismic response when  $R_{d2c}$  increases from 0.1 to 1 is significantly greater than when  $R_{d2c}$  increases from 1 to 3. This suggests that the reduction in seismic response is not proportional to an increase in  $R_{d2c}$ . In addition,  $C_{1,\max}$  is maximum when  $\alpha_2$  is approximately 0.6, which is close to the outrigger elevation that best reduces the seismic response. In addition,  $C_{1,\max}$  is doubled when  $R_{d2c}$  increases from 0.1 to 1 and from 1 to 3. The analysis results indicate that the benefit of reducing seismic responses by increasing  $R_{d2c}$  becomes negligible when  $R_{d2c}$  is too large, however, the  $C_{1,\max}$  keeps increasing at the same rate with increasing  $R_{d2c}$ . Too large value of  $C_{1,\max}$  is not desirable, as it increases the perimeter column sizes. If Fig. 16a is compared with 16b, the seismic response reductions are slightly increased when the value of  $R_{kd}$  changes from 1 to 3. As the upper BRB-outrigger dominates the overall response, the changes in  $\alpha_2$  and  $R_{d2c}$  would affect the overall response more than the changes in  $\alpha_1$  and  $R_{kd}$ .

Figs. 17–20 show the reductions in  $\theta_{\max}$ ,  $\gamma_{\max}$ , and  $M_{c,\max}$  (reduction factor, in percentage) when compared with the structure without outriggers, and the values of  $C_{1,\max}$  for each analytical model when  $R_{d2c} = 1$  and 3 and  $R_{kd} = 1$ . The “×” symbol in Figs. 17–20 indicates the outrigger elevations with the greatest reduction. The shapes of the reduction factor distribution of  $\theta_{\max}$ ,  $\gamma_{\max}$ , and  $M_{c,\max}$  are similar. The reduction factors primarily change with  $\alpha_2$ , and the values are minimum (greatest reduction) when  $\alpha_2$  is between 0.7 and 0.8. The effect of varying  $\alpha_1$  is negligible when  $\alpha_2$  is smaller than 0.4. Even when  $\alpha_2$  is at its approximate optimal elevation (between 0.7 and 0.8), the changes in the reduction factor because of varying  $\alpha_1$  is limited to within 10%. This could suggest that, when  $\alpha_2$  is smaller than 0.4, the presence of the lower outrigger has no contribution in achieving better

seismic performance. Similar findings were also shown in past researches [2,9]. The analysis results shown in Figs. 17–20 indicate that, when  $\alpha_2$  is at its optimal elevation and  $\alpha_1$  is approximately 0.4 to 0.7,  $\theta_{\max}$  and  $\gamma_{\max}$  can be best reduced. The trends of  $\theta_{\max}$  and  $\gamma_{\max}$  distributions with respect to  $\alpha_2$  and  $\alpha_1$  are similar to the 1st mode period trend as shown in Fig. 14. This suggests that the outrigger elevation that has the greatest outrigger effect on the system is also the optimal elevation in order to achieve minimum  $\theta_{\max}$  and  $\gamma_{\max}$ . In addition, when  $\alpha_1$  is approximately 0.2 to 0.4,  $M_{c,\max}$  can be best reduced. It appears that when lower BRB-outrigger is closer to structure base, the  $M_{c,\max}$  can be better reduced. This was also reported in the past research [9]. The  $C_{1,\max}$  results indicate that the perimeter column axial force is maximum when  $\alpha_2$  is approximately 0.5 to 0.7, which is also the optimal elevation of  $\alpha_2$  that best reduces the  $\theta_{\max}$ ,  $\gamma_{\max}$ , and  $M_{c,\max}$  responses. In the models with the same number of stories, the increase in  $R_{d2c}$  from 1 to 3 (increase both the axial stiffness of BRB<sub>1</sub> and BRB<sub>2</sub> by 3 times) only increases the overall reduction by approximately 5%, however, the perimeter column force demand ( $C_{1,\max}$ ) is increased by 50%. For the analysis results in models with different numbers of stories, the reductions are smaller in the taller models that have smaller  $S_{bc2}$  values (as presented in Table 7). Based on the analysis results, a greater value of  $S_{bc2}$  suggests a greater outrigger effect that, therefore, results in smaller reduced seismic response. In summary, the optimal upper outrigger elevations ( $\alpha_2$ ) are approximately 0.7 and 0.8. For the lower outrigger elevation ( $\alpha_1$ ), the optimal  $\alpha_1$  is in the range of 0.4 to 0.7 if the first priority is to mitigate  $\theta_{\max}$  and  $\gamma_{\max}$ , and the optimal  $\alpha_1$  is in the range of 0.2 to 0.4, if mitigating  $M_{c,\max}$  is critical. In order to increase the seismic response reductions, increasing the value of  $S_{bc2}$  when  $\alpha_2 = 0.7$  would be more efficient than increasing the value of  $R_{d2c}$ .

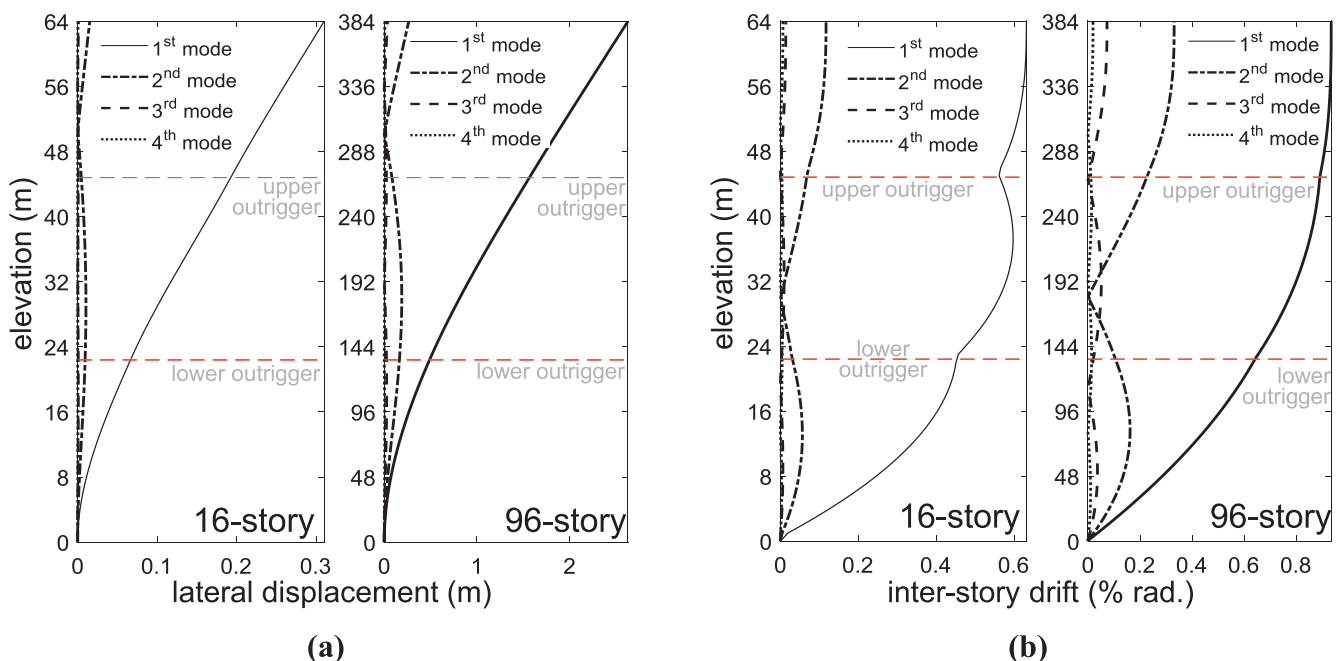


Fig. 13. (a) Lateral displacement and (b) inter-story drift distributions calculated from SA for the 16-story and 96-story models.

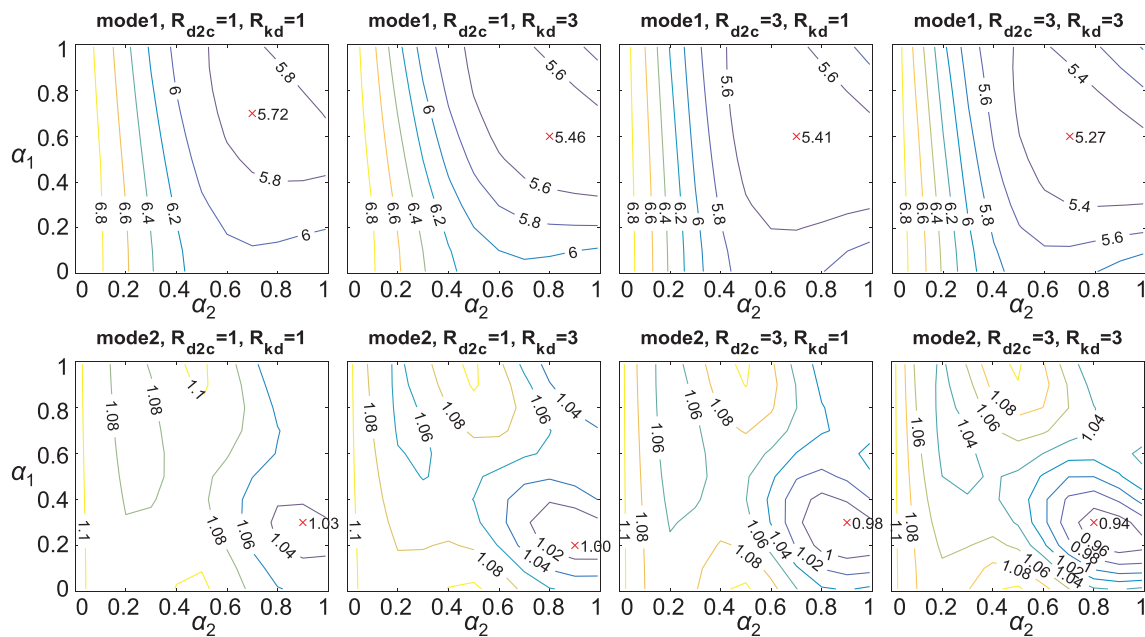


Fig. 14. The 1st and 2nd mode vibration periods of 64-story model when  $R_{kd} = 1$  and 3, and  $R_{d2c} = 1$  and 3 (unit: sec).

Figs. 21–23 show the reductions (in percentage) in  $\theta_{max}$ ,  $\gamma_{max}$ , and  $M_{c,max}$  with respect to  $R_{d2c}$ ,  $S_{bc2}$ , and  $R_{kd}$  for the cases when  $\alpha_2$  is 0.5, 0.7, and 0.9 and when  $\alpha_1$  is 0.3 and 0.6. The additional analysis results calculated from using the 16-storyB, 16-storyC, and 32-storyD models shown in Table 7 are also included in Figs. 21–23. The  $\theta_{max}$  reduction factor plot for  $\alpha_2 = 0.5$ ,  $\alpha_1 = 0.3$ , and  $R_{kd} = 1$  shown in Fig. 21 indicates the distribution of  $S_{bc2}$  and  $R_{d2c}$  data used to create the contour plots. It should be noted that the  $\theta_{max}$  and  $\gamma_{max}$  reduction factor distributions shown in Figs. 21–23 are based on the SA results, and the  $M_{c,max}$  reduction factor distributions are based on the NLRHA results. As can be seen in Figs. 21–23, the shapes of the reduction factor distributions of  $\theta_{max}$ ,  $\gamma_{max}$ , and  $M_{c,max}$  are similar. The greater values of  $R_{d2c}$  and  $S_{bc2}$  suggest a greater outrigger effect indicating a smaller seismic response. However, the rate of increase in the seismic response reduction becomes slower, or even stops, as  $R_{d2c}$  increases under a fixed value of  $S_{bc2}$ . Therefore, the optimal value of  $R_{d2c}$  should be

approximately 0.5 to 1.5. When the value of  $R_{d2c}$  is greater than 1.5, the required BRB axial stiffness increases (increasing the cost of the BRB), however, the reduction in seismic responses becomes less efficient. In addition, if the cases when  $\alpha_2$  varies between 0.5 (Fig. 21), 0.7 (Fig. 22), and 0.9 (Fig. 23) are compared, when  $\alpha_2$  is changed from 0.5 to 0.7, the reductions in  $\theta_{max}$  and  $\gamma_{max}$  increase by approximately 10%, and when  $\alpha_2$  is changed from 0.7 to 0.9, the reductions in  $\theta_{max}$  and  $\gamma_{max}$  increase by approximately 3%, and the changes in the  $M_{c,max}$  reductions are insignificant. However, when  $\alpha_1$  decreases from 0.6 to 0.3, the  $M_{c,max}$  reductions increase by approximately 5% for the cases when  $\alpha_2$  is 0.5 (Fig. 21), and increase by approximately 10% for the cases when  $\alpha_2$  is 0.7 (Fig. 22) and 0.9 (Fig. 23). The analysis results suggest that the optimal upper BRB-outrigger elevation in order to mitigate  $\theta_{max}$  and  $\gamma_{max}$  is approximately 0.7 to 0.9. In addition, if  $\alpha_2$  is within its optimal range, the reduction in  $M_{c,max}$  is optimal when the lower BRB-outrigger is close to the core structure base. When  $R_{kd}$  changes from 1 to 3, the

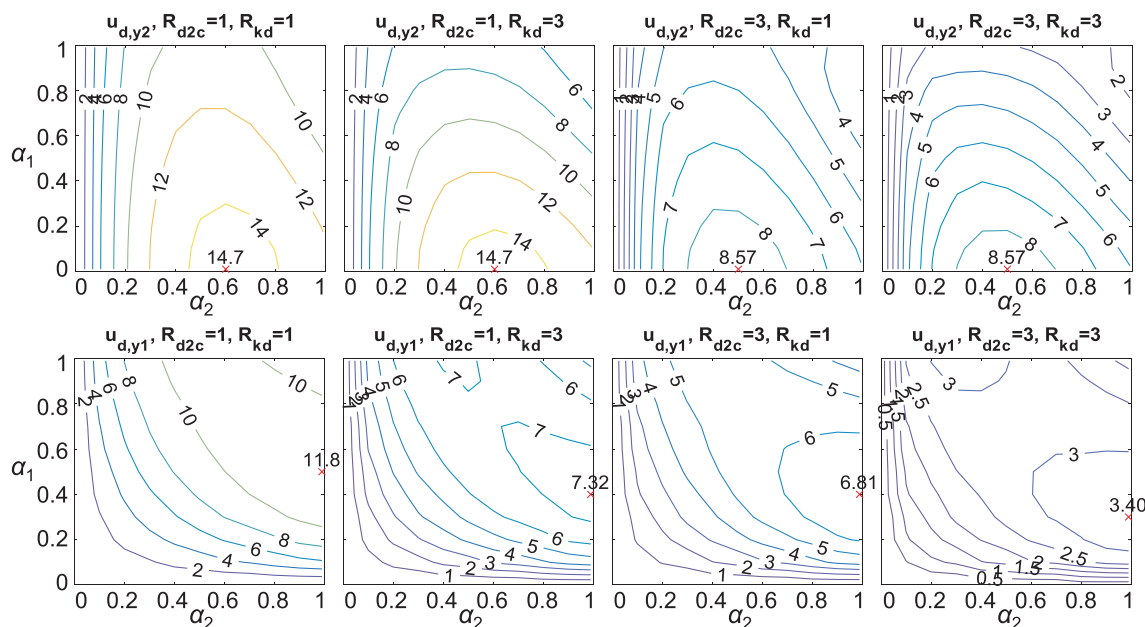


Fig. 15. BRB yield deformations of 64-story model when  $R_{kd} = 1$  and 3, and  $R_{d2c} = 1$  and 3 (unit: mm).

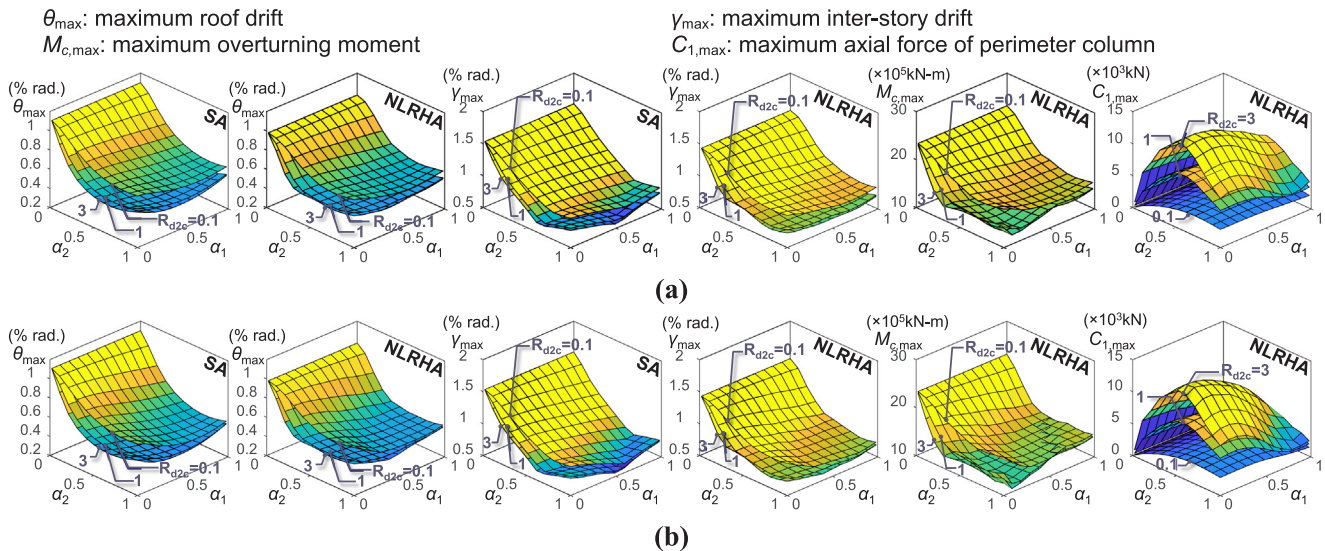


Fig. 16. SA and NLRHA results for 16-story model with (a)  $R_{kd} = 1$  and (b)  $R_{kd} = 3$ .

$\theta_{max}$  and  $\gamma_{max}$  reductions increase by approximately 3% and 5% when  $\alpha_1$  is 0.3 and 0.6, respectively, and the increases in the  $M_{c,max}$  reductions are approximately 5% and 3% when  $\alpha_1$  is 0.3 and 0.6, respectively. Therefore, it appears that the method of increasing  $R_{kd}$  is efficient to reduce  $\theta_{max}$  and  $\gamma_{max}$  when  $\alpha_1$  is approximately 0.6, and to reduce  $M_{c,max}$  when  $\alpha_1$  is approximately 0.3. This also indicates that the abovementioned optimal lower outrigger elevations are approximately 0.4 to 0.7 to minimize  $\theta_{max}$  and  $\gamma_{max}$ , and approximately 0.2 to 0.4 to minimize  $M_{c,max}$ .

Based on the analysis results, the optimal upper ( $\alpha_2$ ) and lower ( $\alpha_1$ ) BRB-outrigger elevations so as to minimize the seismic response are approximately 0.7 to 0.8 and 0.4 to 0.7, respectively. These optimal outrigger elevation values are close to the optimal values presented in the past for the conventional and damped-outrigger systems [2,5–7,9]. The optimal  $\alpha_1$  is also similar to the findings in past studies [2,8,9]. This might indicate that the optimal outrigger elevation values are not significantly affected by the type of outrigger (damped or conventional) or the kind of damper (BRB or viscous damper) employed in the structure. For design practices, selecting the appropriate outrigger elevations should be the first priority as they have the greatest effect on the overall seismic performance.  $S_{bc2}$  should be selected as large as possible as it determines the magnitude of the outrigger effect. The value of  $R_{d2c}$  should be limited between 0.5 and 1.5, as too large  $R_{d2c}$  value increases the cost of the BRB and the additional seismic reduction is insignificant. The lower BRB-outrigger further improves the seismic performance,

and its optimal elevation depends on the design strategy. Placing the lower BRB-outrigger at the elevation where inter-story drift is too large could greatly mitigate the inter-story response. Furthermore, placing the lower BRB-outrigger at  $\alpha_1$  approximately 0.4 to 0.7 could best reduce  $\theta_{max}$  and  $\gamma_{max}$ . If the core structure base overturning moment is critical, the lower BRB-outrigger can be placed at an  $\alpha_1$  of approximately 0.2 to 0.4. The value of  $R_{kd}$  is recommended as 1.0, and it could be used to fine-tune the design as changing it from 1 to 3 only affects the seismic response within 5% to 10% based on the analysis results.

## 6. Design recommendation and example

### 6.1. Design recommendation

Based on the analysis results obtained from the SA and NLRHA, a recommended design flow chart is shown in Fig. 24. For the design practice,  $h$  and  $l_t$  are fixed after the architectural plan and elevation have been determined, and the perimeter column size ( $k_c$ ) and  $EI$  can be roughly designed based on the gravity load and seismic demands. The recommended design procedure is as follows.

- (1) Place the upper outrigger at  $\alpha_2$  around 0.6–0.8 if there is no architectural limitation. Design the outrigger truss so that the  $k_t$  and  $S_{bc2}$  are as large as possible. Select  $R_{d2c}$  between 0.5 and 1.5 and perform SA or NLRHA to obtain the seismic response of the single

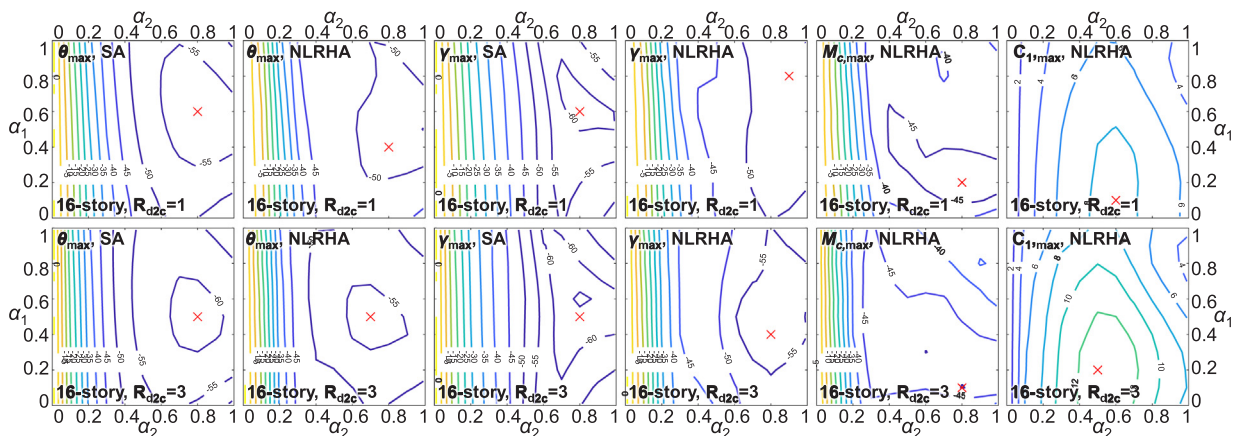


Fig. 17. Reduction factor distributions with respect to outrigger elevations of 16-story model when  $R_{kd} = 1$ .

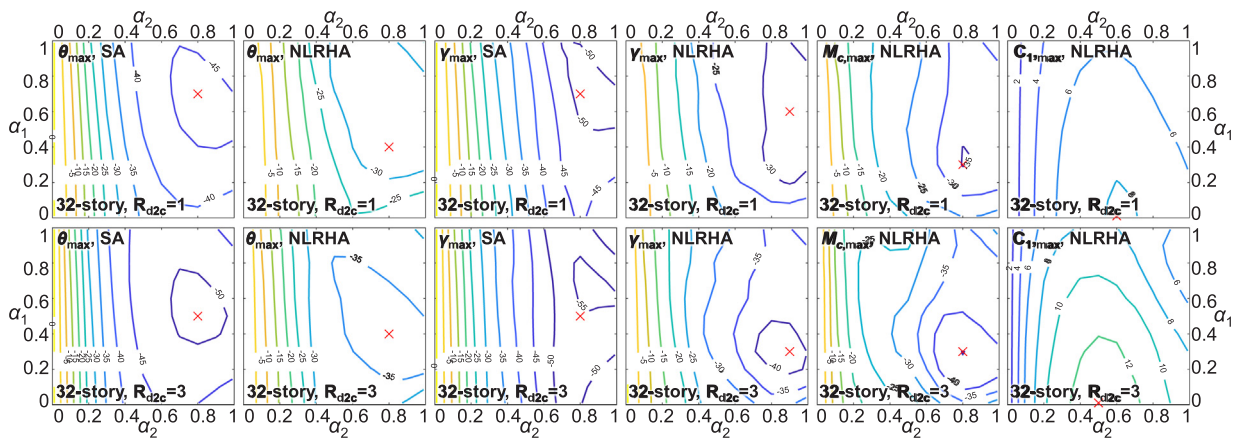


Fig. 18. Reduction factor distributions with respect to outrigger elevations of 32-story model when  $R_{kd} = 1$ .

BRB-outrigger system (upper BRB-outrigger only). Based on the analysis results, place an additional lower BRB-outrigger based on the following conditions:

- A. If  $\theta_{max}$  of the single BRB-outrigger system is too large, place the lower BRB-outrigger with  $R_{kd} = 1$  at  $\alpha_1 = 0.4-0.7$ .
  - B. If  $M_{c,max}$  of the single BRB-outrigger system is too large, place the lower BRB-outrigger with  $R_{kd} = 1$  at  $\alpha_1 = 0.2-0.4$ .
  - C. Place the lower BRB-outrigger with  $R_{kd} = 1$  at the elevation where inter-story drift of the single BRB-outrigger system is too large.
  - D. If the required BRB axial stiffness and outrigger truss flexural stiffness are too large to design the members of the single BRB-outrigger system, place the lower BRB-outrigger at  $\alpha_1 = 0.4-0.7$ , decrease the value of  $R_{d2c}$  to be smaller than 1, and increase the value of  $R_{kd}$  to be greater than 1.
- (2) Calculate the value of  $S_{bc2}$  when  $\alpha_2 = 0.7$  using Eq. (2). Increase the  $S_{bc2}$  (when  $\alpha_2 = 0.7$ ) value to as large as possible while keeping  $\alpha_2$ ,  $k_c$ , and  $k_t$  within acceptable ranges.
  - (3) Select the value of  $R_{d2c}$  to be close to 1, and calculate  $k_{d2}$ .
  - (4) Design the detail, including the yielding deformations of BRB<sub>1</sub> and BRB<sub>2</sub>, based on  $k_{d2}$  and  $R_{kd}$  obtained from the previous steps. Calculate the maximum allowable elastic roof drift limit ( $\theta_r$ ) by performing MPA. If  $\theta_r$  is too small (e.g.  $< 1/750$ ), increase the  $u_{d,y}$ . If  $\theta_r$  is too large (e.g. greater than  $1/350$ ), decrease the  $u_{d,y}$ . Redesign the BRBs until  $\theta_r$  is within a suitable range.
  - (5) Estimate the maximum seismic response by performing the SA or NLRHA. If the maximum seismic response exceeds the limits, proceed to either step (6.1) or step (6.2). Otherwise, proceed to step (7).

- (6.1) If the perimeter column size cannot be changed, increase the value of  $R_{kd}$  to be greater than 1, and repeat from step (4) to redesign the BRB<sub>1</sub>. Then perform the analysis to verify if the seismic responses are reduced.
- (6.2) If the perimeter column size can be changed, increase the value of  $S_{bc2}$  (when  $\alpha_2 = 0.7$ ) by increasing  $k_c$ . Repeat from step (3) with the updated  $k_c$ .
- (7) Check the maximum axial force demand of the perimeter column. If the demand-to-capacity ratio (DCR) of the perimeter column is greater than 1.0, increase the size of the perimeter column. Repeat from step (4) to redesign BRB<sub>1</sub> and BRB<sub>2</sub> with updated  $k_c$ . If the DCR of perimeter column is smaller than 1.0, then the design is finished.

### 6.2. Design example

The design recommendation assists engineers by providing a clear procedure to design the dual BRB-outrigger system. In addition, the design charts, which are based on analysis results, provide engineers with a quick and efficient way to select the lower BRB-outrigger elevation in order to achieve the desired seismic response. The use of design charts is illustrated by a 48-story model ( $h = 192$  m) example. The outrigger truss span ( $l$ ) of the 48-story model is 20 m, and the mass is 1125 ton on each floor. The perimeter column size is Box  $1700 \times 1700 \times 100$  mm made of SN490 grade steel with infill concrete with a compressive strength of 10000 psi (70 MPa). The values of  $EI$  and  $k_c$  are  $4.1 \times 10^{10}$  kN-m<sup>2</sup> and  $6.7 \times 10^5$  kN/m, respectively. The single BRB-outrigger design results are  $\alpha_2 = 0.7$ ,  $S_{bc2} = 1.26$ ,  $R_{dt} = 0.1$ , and  $R_{d2c} = 1$ . If the perimeter column size ( $k_c$ ) and the upper BRB-elevation

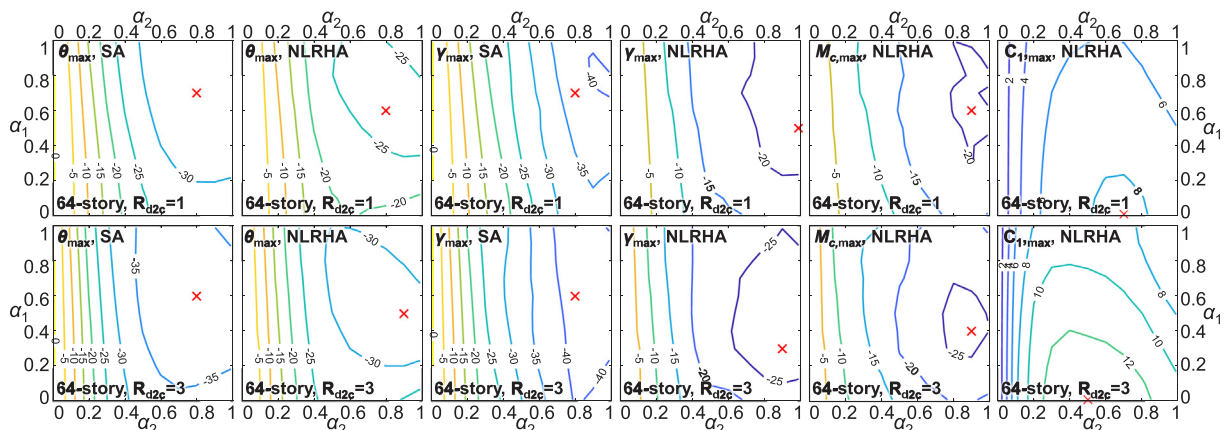


Fig. 19. Reduction factor distributions with respect to outrigger elevations of 64-story model when  $R_{kd} = 1$ .

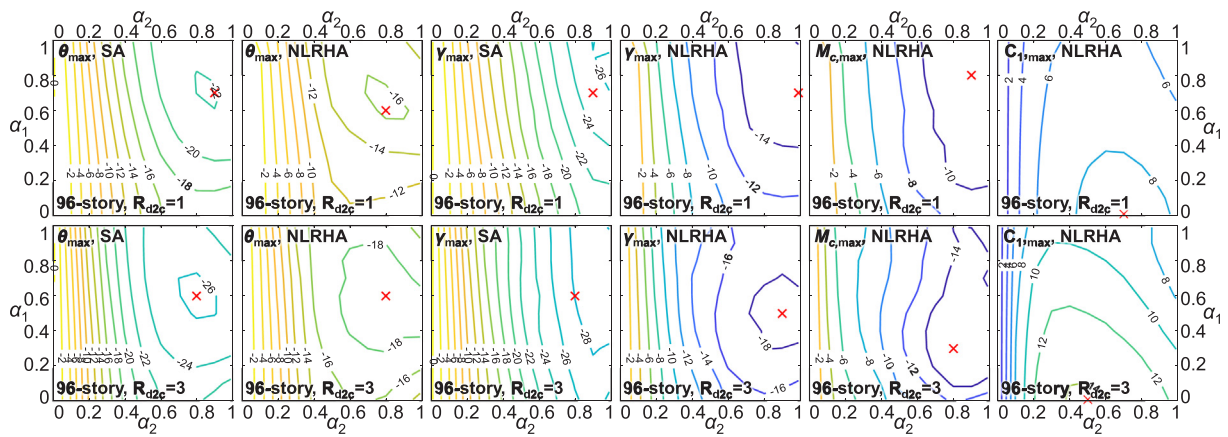


Fig. 20. Reduction factor distributions with respect to outrigger elevations of 96-story model when  $R_{kd} = 1$ .

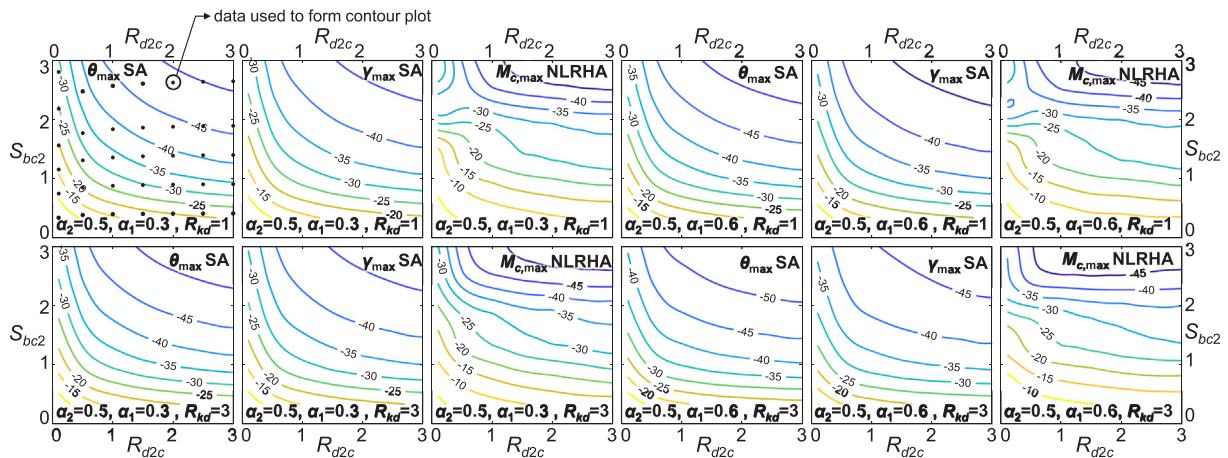


Fig. 21. Reduction factors distribution with respect to  $R_{d2c}$  and  $S_{bc2}$  when  $\alpha_2$  is 0.5.

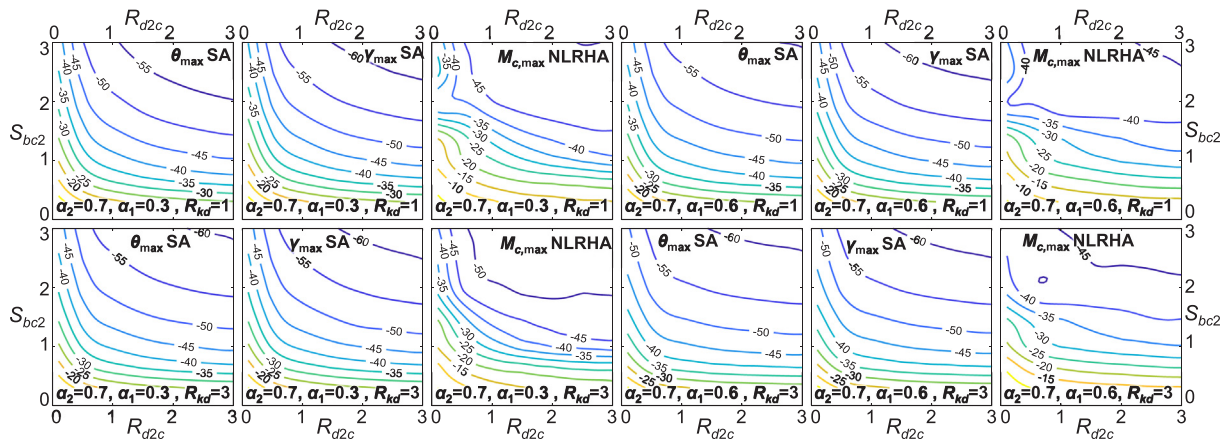


Fig. 22. Reduction factors distribution with respect to  $R_{d2c}$  and  $S_{bc2}$  when  $\alpha_2$  is 0.7.

( $\alpha_2$ ) are not allowed to change, the design charts for selecting a proper lower BRB-outrigger elevation are shown in Fig. 25, which also shows the design charts for  $R_{d2c} = 1, 2,$  and  $3$  and  $R_{kd} = 0.5$  and  $1$ . Each design chart shows the reduction factor distributions with respect to  $S_{bc2}$  and  $\alpha_1$ . Based on the design charts,  $\theta_{max}$  and  $\gamma_{max}$  are best reduced when  $\alpha_1$  is in the range of  $0.7$  and  $0.8$ , and  $M_{c,max}$  can be best reduced when  $\alpha_1$  is in the range of  $0.3$  and  $0.4$ . If the  $R_{d2c}$  is kept constant at  $1$ ,  $R_{kd}$  is kept constant at  $1$ , and the lower BRB-outrigger is kept at its optimal elevation,  $\theta_{max}$  and  $\gamma_{max}$  can be reduced by  $5\%$  and  $M_{c,max}$  can be reduced by  $9\%$  compared with the original single BRB-outrigger solution (when

$\alpha_1 = 0$  in Fig. 25). If the  $R_{d2c}$  value can be increased to  $2$  or  $3$  (2 or 3 times the BRB stiffness in the single BRB-outrigger design), the reductions can be increased by  $5\%$  or  $7\%$ , respectively. In addition, if the  $R_{kd}$  value increases from  $0.5$  to  $1$ , the reduction factors can be increased by approximately  $3\%$  to  $5\%$ . Fig. 26 shows the SA and NLRHA results for the core structure (Core) and single BRB-outrigger (Single) cases, and when an additional lower BRB-outrigger is placed at  $\alpha_1 = 0.3$  (Dual) and  $R_{kd} = 1$ . The fundamental vibration periods for the Core, Single, and Dual models are  $5.48, 4.25,$  and  $4.02$  s, respectively. The NLRHA results in this section are obtained from six (one artificial and five

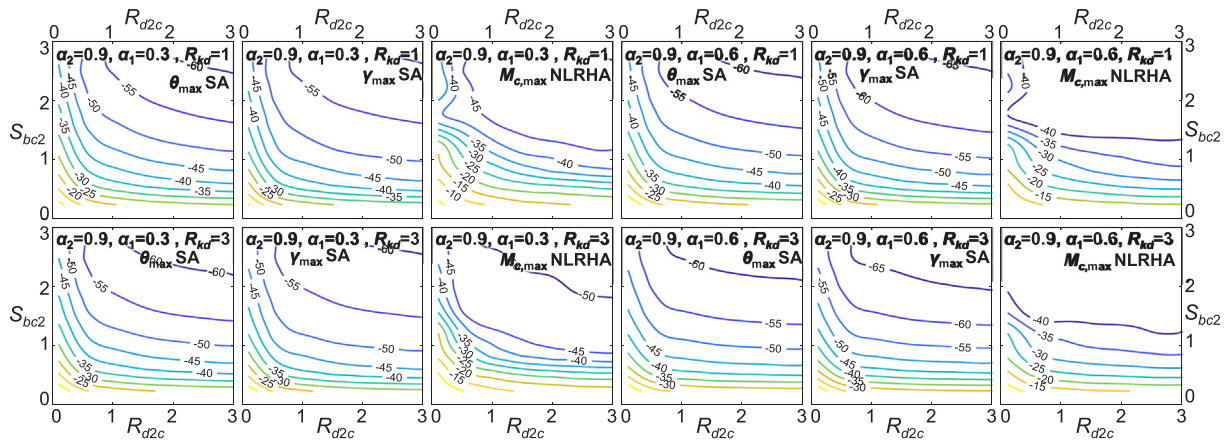


Fig. 23. Reduction factors distribution with respect to  $R_{d2c}$  and  $S_{bc2}$  when  $\alpha_2$  is 0.9.

observed) ground motions. Table 9 presents the reduction factors for the Dual models compared with the Core and Single models. The reduction factors obtained from the design charts and the SA procedure are in good agreement. The NLRHA results suggest that the reduction factors vary with ground motions. The ratio of the energy dissipated by BRBs to the total input energy ( $E_{BRB}$ ) shown in Fig. 26 indicates that ground motion 4 exhibits the smallest  $E_{BRB}$  value. The low BRB energy dissipation efficiency (low  $E_{BRB}$  value) could help in explain the  $\theta_{max}$  increase if compared to the Single model under ground motion 4. The additional lower BRB-outrigger stiffens the system and could increase the seismic demand, but the low BRB energy dissipation efficiency (low  $E_{BRB}$  value) could not compensate for the amplified response because of the greater seismic demands. The amount of energy dissipated by the BRB-outrigger systems depends on the seismic intensity of the input ground motion. The ground motions with greater seismic intensity lead to larger energy dissipation by the BRB-outrigger systems. In addition, the Dual models generally produce greater energy dissipation amount than the Single models. Fig. 27 shows the maximum inter-story drift distributions throughout the building height. It should be noted that, as

the core structure is assumed to deform elastically, the BRB-outriggers and system inherent damping effect are the energy dissipation mechanism. If the yield inter-story drift is 0.5% rad., the core structure stays in elastic deformation during the El Centro, Taft, and Tohoku earthquakes, and the BRB-outrigger dissipates approximately 20% to 30% of the total input energy. The core structure appears to yield during the BCJ-L2, ChiChi, and KobeJMA earthquakes. Although the BRB-outriggers dissipate 40% to 70% of total input energy during the BCJ-L2, ChiChi, and KobeJMA earthquakes, the core structure needs to be reinforced to keep it in elastic. In case of allowing partial plasticity in the core structure, the ratio of energy dissipated by the BRB-outriggers will be reduced. Based on the analysis results of the design example, it appears that the reduction factors obtained from the design chart and the SA are the maximum possible values. Both the single and dual BRB-outrigger systems effectively reduce the seismic response compared to the structure without BRB-outriggers, and the dual BRB-outrigger generally performs better than single BRB-outrigger. For design practices, the design charts provide engineers an efficient alternative to time-consuming iterative tasks by presenting a rough response in the

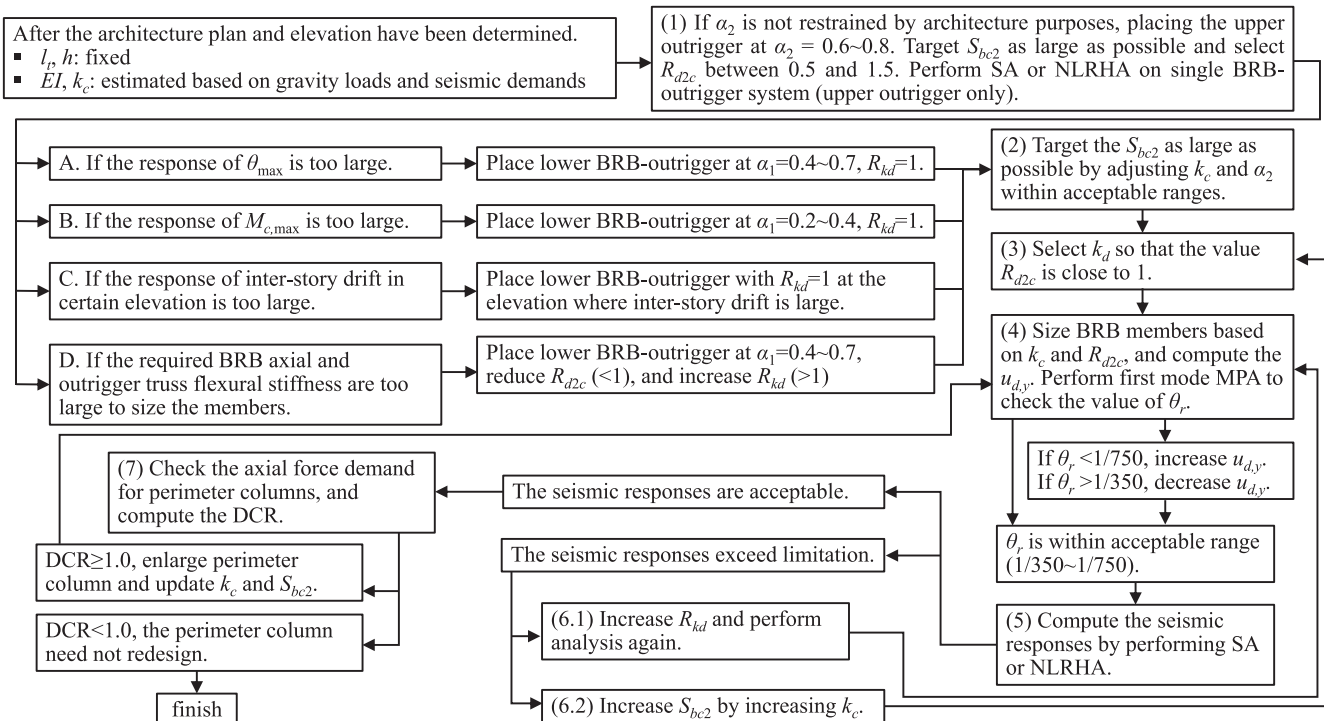


Fig. 24. Flow chart of design recommendation.

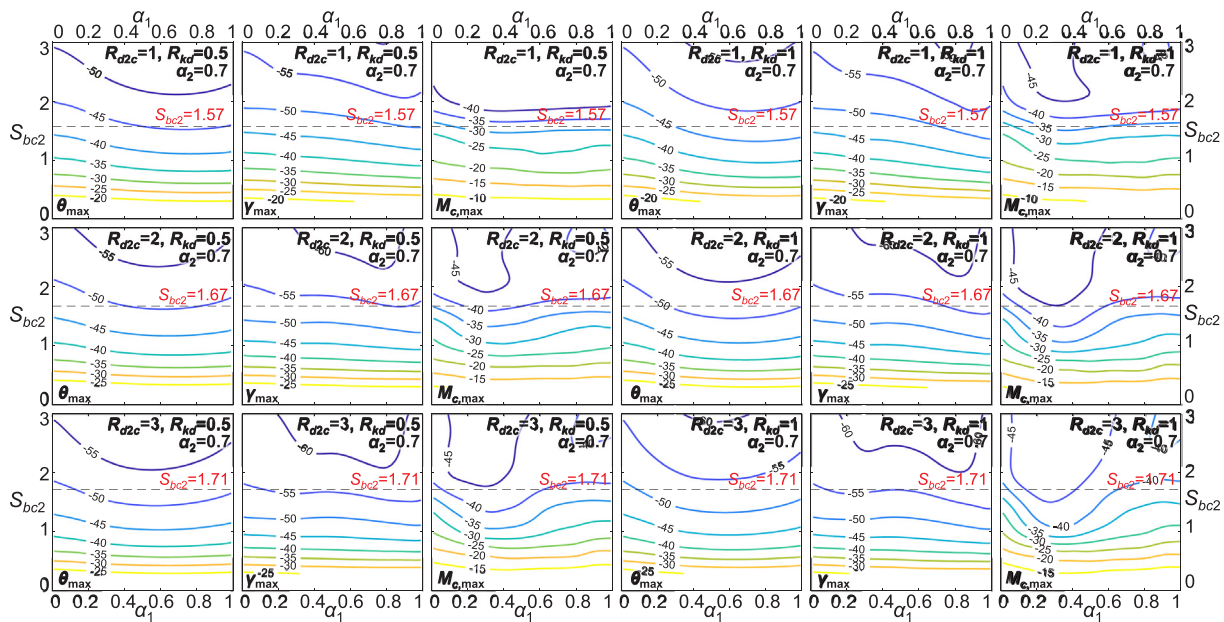


Fig. 25. Design charts for design example.

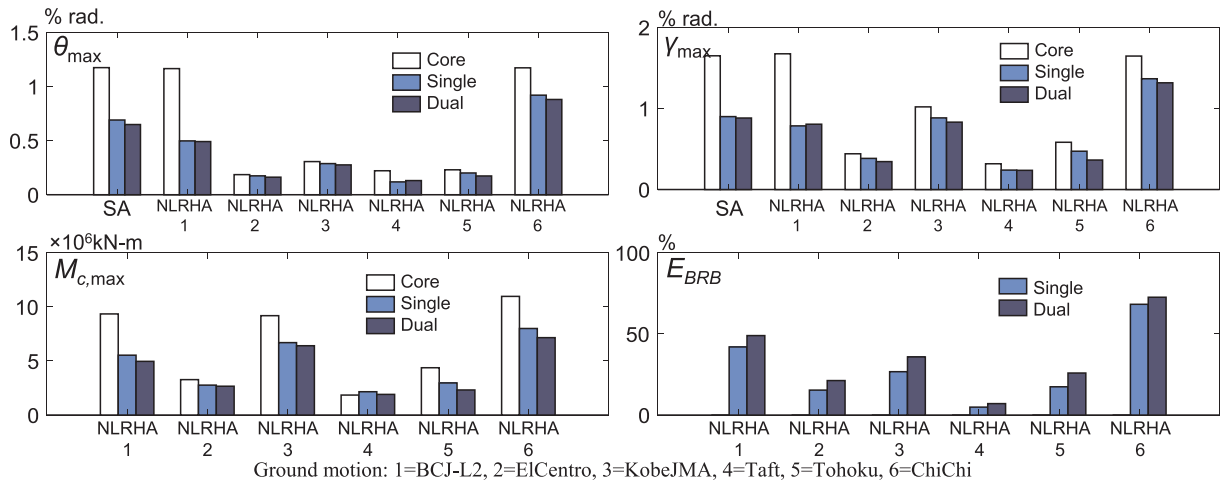


Fig. 26. Seismic responses of design example model.

Table 9  
Reduction factors of dual BRB-outrigger design example.

Reduction factor type	Compare to	Design chart	SA	NLRHA					
				1	2	3	4	5	6
$\theta_{max}$	Core	-47%	-45%	-58%	-13%	-10%	-41%	-25%	-25%
	Single	-	-6%	-1%	-7%	-4%	+10%	-14%	-4%
$\gamma_{max}$	Core	-48%	-47%	-52%	-22%	-18%	-26%	-38%	-20%
	Single	-	-2%	+3%	-10%	-6%	-1%	-23%	-4%
$M_{c,max}$	Core	-35%	-	-47%	-19%	-30%	+3%	-47%	-35%
	Single	-	-	-10%	-4%	-4%	-11%	-22%	-11%
PGA (gal)				356	342	821	176	258	439

Ground motion: 1 = BCJ-L2, 2 = ElCentro, 3 = KobeJMA, 4 = Taft, 5 = Tohoku, 6 = ChiChi.

preliminary design stage. However, it is suggested that the detail design and seismic response should be obtained from rigorous analysis processes using a more refined MBM model.

7. Conclusions

This study proposed a simplified model and SA procedure to

evaluate the seismic response for buildings with multiple BRB-outrigger systems. The optimal outrigger elevations, the optimal relationships between the two BRBs' axial stiffness, perimeter column axial stiffness, and flexural rigidity of the core structure in order to best reduce seismic response of the dual BRB-outrigger system are investigated. Based on the analysis results, the following conclusions were drawn:

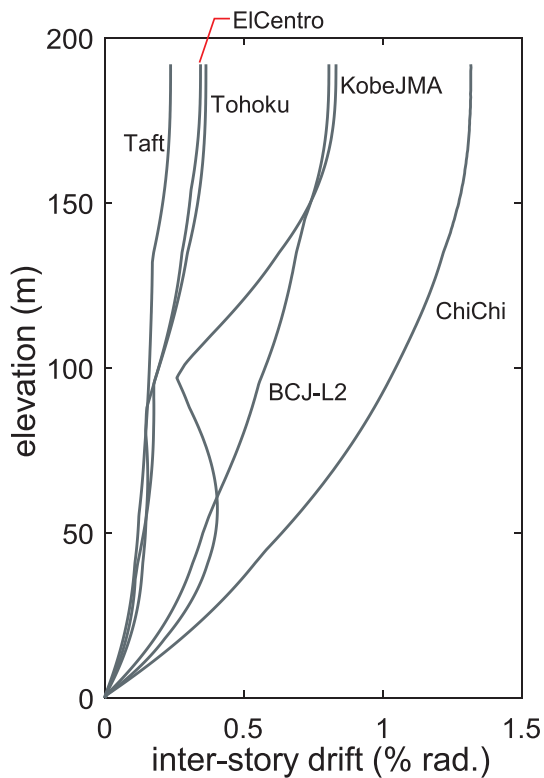


Fig. 27. The maximum inter-story drift distributions throughout building height of the 48-story example model.

- (1) A good agreement in the modal analysis results obtained from the DM and MBM models indicate that the DM model is a good representation of the MBM model. The similar NLRHA results obtained from the DM and MBM models suggest that the DM model well represent the single and dual BRB-outrigger systems. The DM model was used to perform the MPA in order to study the inelastic behavior of the multi BRB-outrigger system in the SA procedure. The DM model was also used to perform the NLRHA in order to verify the SA results.
- (2) The SA procedure using the equivalent damping ratio to evaluate the hysteretic responses of the BRBs. The responses from the first four modes were considered in the SA. The results obtained from SA and NLRHA exhibited similar trends.
- (3) For the dual BRB-outrigger systems, the parameters  $\theta_{\max}$ ,  $\gamma_{\max}$ , and  $M_{c,\max}$  primarily changed with the upper BRB-outrigger elevation ( $\alpha_2$ ). The upper BRB-outrigger dominates the seismic response, and the presence of additional lower BRB-outrigger further improved the seismic response by reducing  $\theta_{\max}$ ,  $\gamma_{\max}$ , and  $M_{c,\max}$ .
- (4) By utilizing the BRB-outrigger system, the optimal  $\alpha_2$  and  $\alpha_1$  in

order to minimize  $\theta_{\max}$  and  $\gamma_{\max}$  were 0.7 to 0.8 and 0.4 to 0.7, respectively. The value of  $M_{c,\max}$  could be best reduced when  $\alpha_1$  was between 0.2 and 0.4. In addition, the lower BRB-outrigger could be placed at the elevation where the inter-story drift ratio was too large to mitigate the excessive inter-story drift response. The optimal  $\alpha_1$  and  $\alpha_2$  were not significantly affected by the values of  $S_{bc2}$ ,  $R_{d2c}$ , and  $R_{kd}$ . However,  $C_{1,\max}$  may increase most when  $\alpha_2$  was between 0.5 and 0.7.

- (5) Increasing  $R_{d2c}$  could reduce  $\theta_{\max}$ ,  $\gamma_{\max}$ , and  $M_{c,\max}$ , but the rate of reduction decreased, or even stopped, with increasing  $R_{d2c}$ . The optimal  $R_{d2c}$  should be approximately 0.5 to 1.5.

#### Acknowledgement

This research was supported by Japan Society for the Promotion of Science (JSPS) KAKENHI Grand number 18J15047.

#### References

- [1] Ali M, Moon KS. Structural developments in tall buildings: current trends and future prospects. *Architect Sci Rev* 2007;50(3):205–23.
- [2] Smith S, Salim I. Parameter study of outrigger-braced tall building structures. *J Struct Divis* 1981;107(10):2001–14.
- [3] Viise J, Ragan P, Swanson J. BRB and FVD alternatives to conventional steel brace outriggers. Proceedings of the CTBUH Shanghai conference. 2014. p. 691–9.
- [4] Smith R, Willford M. The damped outrigger concept for tall buildings. *Struct Des Tall Special Build* 2007;16(4):501–17.
- [5] Huang B, Takeuchi T. Dynamic response evaluation of damper-outrigger system with various heights. *Earthquake Spectra* 2017;33(2):665–85.
- [6] Chen Y, McFarland D, Wang Z, Spencer B, Bergman L. Analysis of tall building with damped outriggers. *J Struct Eng* 2010;136(11):1435–43.
- [7] Tan P, Fang C, Zhou F. Dynamic characteristics of a novel damped outrigger system. *Earthquake Eng Eng Vibrat* 2014;13(2):293–304.
- [8] Morales-Beltran M, Turan G, Dursun O, Nijse R. Energy dissipation and performance assessment of double damped outriggers in tall buildings under strong earthquakes. *Struct Des Tall Special Build* 2018. <https://doi.org/10.1002/tal.1554>.
- [9] Wu JR, Li QS. Structural performance of multi-outrigger-braced tall buildings. *Struct Des Tall Special Build* 2003;12(2):155–76.
- [10] Xing L, Zhou Y, Aguaguina M. Optimal vertical configuration of combined energy dissipation outriggers. *Struct Des Tall Special Build* 2018. <https://doi.org/10.1002/tal.1579>.
- [11] Willford M, Smith R. Performance based seismic and wind engineering for 60 story twin towers in Manila. Proceedings of the 14th world conference on earthquake engineering, Beijing, China. 2008.
- [12] Takeuchi T, Wada A. Buckling-restrained braces and application. Tokyo, Japan: Japan Society of Seismic Isolation (JSSI); 2017.
- [13] Joseph L, Gulec K, Schwaiger J. Wilshire Grand: outrigger designs and details for a high seismic site. *Int J High-Rise Build* 2016;5(1):1–12.
- [14] McKenna F. Object oriented finite element programming frameworks for analysis, algorithm and parallel computing PhD. thesis Berkeley: University of California; 1997.
- [15] Newmark M, Rosenblueth E. Fundamentals of earthquake engineering. Englewood Cliffs, N.J., USA: Prentice-Hall Inc; 1971.
- [16] Chopra A, Goel R. A modal pushover analysis procedure for estimating seismic demands for buildings. *Earthquake Eng Struct Dyn* 2002;31(3):561–82.
- [17] Kasai K, Fu Y, Watanabe A. Passive control system for seismic damage mitigation. *J Struct Eng* 1998;124(5):501–12.
- [18] <https://www.bcj.or.jp/> The Building Center of Japan.